Report No. UT- 07.02

TIME-DEPENDENT EFFECTS AND VALIDATION FROM MONITORING OF POST-TENSIONED SPLICED GIRDERS AND DECK JOINTS

Final Report

Prepared For:

Utah Department of Transportation
Research and Development Division

Submitted By:

University of Utah
Department of Civil & Environmental Engineering

Authored By:

Chris P. Pantelides
Brant W. Saxey
Joseph Emerson
Lawrence D. Reaveley

December 2006

DISCLAIMER

The Contents of this report reflect the view of the authors, who are responsible for the facts and accuracy of the data presented herein. The contents do not necessarily reflect the official views or policies of the Utah Department of Transportation (UDOT).

1. Report No.	2. Government Accession No.	3. Recipient's Catalog No.
UT- 07-02		

4. Title and Subtitle	5. Report Date
TIME-DEPENDENT EFFECTS AND VALIDATION FROM MONITORING OF POST-TENSIONED SPLICED GIRDERS AND DECK JOINTS	DECEMBER, 2006
	6. Performing Organization Code

7. Author	8. Performing Organization Report No.
Chris P. Pantelides Brant W. Saxey Joseph Emerson Lawrence D. Reaveley	CVEEN -06/2

9. Performing Organization Name and Address	10. Work Unit No.
University of Utah Department of Civil & Environmental Engineering 112 South Central Campus Drive Salt Lake City, Utah 84112-0561	11. Contract or Grant No.

12. Sponsoring Agency Name and Address	13.Type of Report & Period Covered
Utah Department of Transportation 4501 South 2700 West Salt Lake City, Utah 84114-8410	FINAL
	14. Sponsoring Agency Code

15. Supplementary Notes

Prepared in cooperation with the Utah Department of Transportation or U.S Department of Transportation, Federal Highway Administration.

16. Abstract

This project report summarizes the results of monitoring a post-tensioned spliced girder bridge in Salt Lake City. This report describers the monitoring of the 4500 South Bridge on Interstate 15. The north-bound bridge consists of eight post-tensioned, spliced, precast concrete girders, having three segments each, for a single clear span of 61.443 m (201 ft - 7 in.). Four girders and portions of the bridge deck and parapet wall have been instrumented and monitored for approximately four years. Data recorded from the bridge included concrete strain at selected girder locations, as well as post-tensioned girder losses through eight load cells, and girder deflections for one of the girders through surveys. The actual losses at midspan in the girder being monitored, including time-dependent losses and anchorage seating and friction losses, were on average 14.5% of the initial post-tensioning forces; the absolute upward midspan deflection was 0.15% of the clear span, and the two splice points were deflecting in an almost identical manner indicating excellent girder/splice performance. Analytical procedures are compared to experimental measurements of the losses of the post-tensioned spliced precast concrete girder being monitored. The assumed losses in design were very close to those observed and the design methodology for incorporating losses is found to be adequate. Shrinkage and creep tests, performed on concrete used in constructing the post-tensioned spliced, precast concrete girders, were used to obtain the ultimate creep coefficient and ultimate shrinkage strain. LVDT measurements at the cold joints show that the cold joints are in good health. The abutment movements and rotations were found to be small. The vertical deflections of the post-tensioned girders were measured due to thermal gradients and were compared to AASHTO predicted deflections. General recommendations for using spliced-girder post-tensioned bridges in future projects are provided.

17. Key Words	18. Distribution Statement	23. Registrant's Seal
Concrete Bridges, Creep, Deflections, Health Monitoring, Post-tensioning, Shrinkage, Spliced Girders, Time-Dependent Losses	UDOT Research Division 4501 south 2700 West-box 148410 Salt Lake City, Utah 84114	

19. Security Classification	20. Security Classification	21. No. of Pages	22. Price
Unclassified	Unclassified	70	

ACKNOWLEDGEMENTS

The authors would like to thank the following individuals for their support thought the project and wish to acknowledge Mr. Doug Anderson, Mr. Daniel Hsiao, Mr. Stan Burns, and Mr. Ray Cook of the Utah Department of Transportation (UDOT) for their help with coordinating between UDOT and University of Utah.

The authors would like to acknowledge the contribution of Wasatch Constructors and VSL Inc.

In addition, they acknowledge the assistance of Thomas Weinmann of CTL, Inc. The authors also acknowledge Professor Steven Bartlett and the following individuals and students from the University of Utah: Mark Bryant, Daniel Alire, Jason Rapich, Clifton Farnsworth, Jaron Reay, Yasuteru Okahashi, and Jeff Duffin.

TABLE OF CONTENTS

LIST OF TABLES

LIST OF FIGURES

LIST OF FIGURES

EXECUTIVE SUMMARY

This project report summarizes the results of monitoring a post-tensioned spliced girder bridge in the Salt Lake City area. This report describers the monitoring of the 4500 South Bridge on Interstate 15. As part of the reconstruction of Interstate 15 through Salt Lake City, Utah, the bridge over 4500 South Street was built using a segmental section of the new WSDOT precast concrete deep girder. The north-bound bridge consists of eight post-tensioned, spliced, precast concrete girders, having three segments each, for a single clear span of 61.443 m (201 ft - 7 in.). Four girders and portions of the bridge deck and parapet wall have been instrumented and monitored for approximately four years. Data recorded from the bridge included concrete strain at selected girder locations, as well as post-tensioned girder losses through eight load cells, and girder deflections for one of the girders through surveys. At the end of the monitoring period, the actual losses at midspan in the girder being monitored, including time-dependent losses and anchorage seating and friction losses, were on average 14.5% of the initial post-tensioning forces; the absolute upward midspan deflection was 0.15% of the clear span, and the two splice points were deflecting in an almost identical manner indicating excellent girder/splice performance. Analytical procedures are presented for determining post-tensioning losses of a typical spliced, precast concrete girder used at the 4500 South Bridge on I-15. The analysis procedure specified in the AASHTO LRFD Bridge Design Specifications is used. The analytical method is compared to experimental measurements of the losses of the post-tensioned spliced precast concrete girder being monitored. The time-dependent method predicts the measured losses with sufficient accuracy at the abutments and at midspan. The assumed losses in design were very close to those observed and the design methodology for incorporating losses is found to be adequate. Shrinkage and creep tests, performed on concrete used in constructing the post-tensioned spliced, precast concrete girders, were used to obtain the ultimate creep coefficient and ultimate shrinkage strain. LVDT measurements at the cold joints under the deck in truck load tests and from ambient measurements were obtained which show that the cold joints are in good health. The abutment movements and rotations were obtained from measurements carried out by surveys and were found to be small. The vertical deflections of the post-tensioned girders under monitoring were measured due to thermal gradients and were compared to AASHTO predicted deflections. The AASHTO method was found to be reliable for prediction of deflections due to thermal gradients for spliced post-tensioned girder bridges. Finally, general recommendations for using spliced-girder post-tensioned bridges in future projects are provided.

MONITORING OF POST-TENSIONED SPLICED GIRDERS AND DECK JOINTS

As part of the reconstruction of Interstate 15 through Salt Lake City, Utah, the bridge over 4500 South Street was built using a segmental section of the new WSDOT precast concrete deep girder. The north-bound bridge consists of eight post-tensioned, spliced, precast concrete girders, having three segments each, for a single clear span of 61.443 m (201 ft - 7 in.). Four girders and portions of the bridge deck and parapet wall have been instrumented and monitored for four approximately years. Data recorded from the bridge included concrete strain at selected girder locations, as well as post-tensioned girder losses and girder deflections for one of the girders. This section describes the monitoring effort regarding the post-tensioning losses observed and comparisons to AASHTO predictions and the initial design predictions. The present section also presents design recommendations for coefficients to be used in creep and shrinkage calculations. In addition, the section describes recommendations on use of precast concrete panels for constructing the deck, with emphasis on cold joints between the panels, a comparison of girder deflections to AASHTO predictions related to temperature gradient variations, and general recommendations for using spliced-girder post-tensioned bridges in future projects.

1. INTRODUCTION

Designers have experienced limitations when using existing precast, prestressed concrete I-girders in continuous span bridges. The NU girder was developed by Geren and Tadros (1994) to overcome these limitations and to take advantage of recent advances in precast concrete production technology. The NU girder was developed originally for optimal performance in a two-span bridge with full-length continuity post-tensioning. The development of the NU girder series, and performance comparisons with several existing standard girder shapes were presented. Abdel-Karim and Tadros (1992) described how splicing of I-girders provided a convenient means of extending the span of existing AASHTO and PCI shapes beyond their conventional span ranges; they concluded that longer and structurally more efficient spans could be built and, in some cases, the required number of piers could be reduced.

New deep precast, prestressed concrete girder sections were adopted as Washington State Department of Transportation (WSDOT) standards. These girders, reported by Seguirant (1998), were deeper and span further than those previously adopted by WSDOT standards; in some cases, the sections allowed for wider spacings and fewer girder lines. Wollmann et al. (2003) reviewed and demonstrated the age-adjusted concrete modulus approach for the time-dependent analysis of spliced precast concrete girder composite bridges. This approach allows designers to take advantage of the higher concrete strength at the time of post-tensioning, and a resulting reduction in creep and shrinkage strains when determining prestressing losses for design.

The cost-effectiveness of bulb-tee girders for bridge construction was presented by Ronald (2001), including the use of high strength concrete to extend span length. The structural system used precast, pretensioned bulb-tee girders, field spliced and post tensioned in two stages for a continuous composite structural system spanning three to five spans; it was concluded that the structural system could be economically used for spans up to 97.536 m (320 ft). Research on monitoring losses in post-tensioned spliced girders is limited. The Interstate 15 reconstruction in Salt Lake City, in preparation for the 2002 Olympic Winter Games, included 81 prestressed concrete I-girder bridges. For sixteen long-span bridges along the I-15 corridor, the segmental section W24PTMG of the new WSDOT deep girder series was used. The 4500 South Bridge at Interstate 15, which is a spliced girder bridge was selected for monitoring post-tensioning losses.

2. EXPERIMENTAL OVERVIEW

The ultimate goal of the research was health monitoring and performance evaluation of the Interstate 15 post-tensioned, spliced, precast concrete girder bridge at 4500 South. The study period for monitoring the post-tensioned tendons covered 1342 days, from the time the tendons were tensioned on April 27, 2000, until December 31, 2003. Instrumentation of two spliced girders began on December 13, 1999 while the girders were constructed; it included the placement of vibrating wire strain gauges at strategic locations in both girders. The girders were cast on December 15, 1999 and December 20, 1999 and taken to the site in February of 2000. Post-tensioning of the tendons took place on April 27 and 28, and May 1, 2000. After post-tensioning, the tendons were grouted on May 4, 2000; the south abutment end-diaphragm was placed on May 23, 2000, the north abutment end-diaphragm was placed on June 3, 2000, and the bridge was opened to traffic on December 17, 2000. Strain gauge and load cell readings were recorded from the time of jacking; initially, data were collected manually using digital readout instruments; subsequently, an automated data acquisition system was installed for recording data every 15 minutes from each sensor.

Each of the two bridges of the 4500 South and I-15 overpass consisted of eight girders with a single clear span of 61.443 m (201 ft-7 in.) and a skew angle of 8° 03' 41" as shown in Figure 1. Each spliced girder consisted of three segments, with the outer segments measuring 18.782 m (61 ft-7 in.) and the center segment 24.275 m (79 ft-8 in.). The end segments were embedded a distance of 0.500 m (1 ft -8 in.) in the end-abutments and thus the abutments are considered semi-integral. Two reinforced concrete diaphragms in the transverse direction, 302 mm (12 in.) wide each, and of the same height as the girders, connected the three segments of the spliced girders. The segments of each girder were joined by post-tensioned tendons, the diaphragms at the two splice points, and the north and south end-abutments; the tendons were bonded. Each girder is supported at the two end-abutments by an expansion bearing.

Measured data included strain readings from horizontally and vertically oriented vibrating wire strain gauges, located in the girders and parapet wall for a total of 62 gauges**.** Two girders were instrumented with vibrating wire strain gauges at the plant. The eastern-most girder was instrumented along its whole length. Three segments of the second instrumented girder were placed in three different girder lines to compare the performance of the splices. Strain gauge data were used to investigate the performance of the girders, particularly the splices. Four tiltmeters were installed to observe continuity of the splices and out-of-plane rotation of the girders. Load cell readings were used to measure post-tensioning losses on the eastern-most girder, from load cells attached to the four tendons at the north and south girder ends at the time of post-tensioning, for a total of eight load cells. Vibrating wire strain gauges located at midspan were used to evaluate the tendon forces by correlating measured strain with tendon force.

After bridge construction was completed, seven survey points were established on the eastern-most girder to measure deflections; the seven points were evenly spaced with the fourth point at the bridge midspan, one point above each support, and two between each support and midspan. The data was collected continuously from initial bridge construction through the end of December 2003; this provided information regarding the effects of construction and post-tensioning processes, and changes that occurred in the post-tensioned precast concrete girder bridge over an extended period of time.

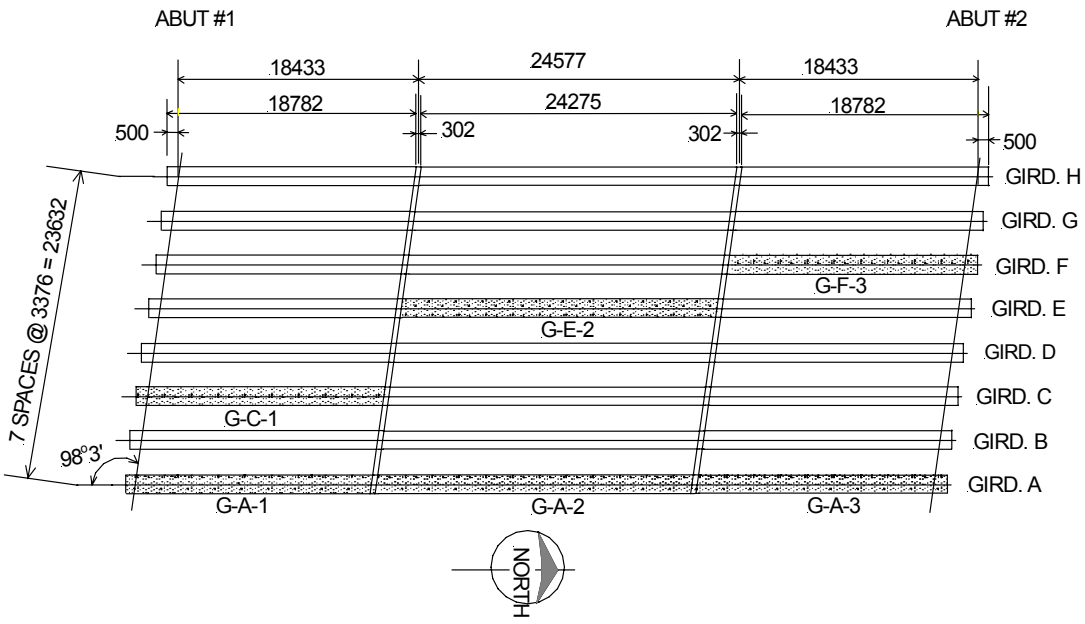

Figure 1. Girder framing plan showing instrumented girder segments (1 in. = 25.4 mm).

3. DESCRIPTION OF POST-TENSIONED SPLICED GIRDER SYSTEM

The girders under investigation were cast segmentally in three segments on December 15 and 20, 1999. Girder A, which was later instrumented with eight load cells, is shown in Figure 2 directly prior to casting. The vertical profile of the south segment of Girder A, denoted as G-A-1 in Figure 1, is shown in Figure 3; the four tendon profile details are given in Table 1. The vertical profile of the middle segment of Girder A, denoted as G-A-2 in Figure 1, is shown in Figure 4; the four tendon profile details are given in Table 2. The vertical profile of the north segment of Girder A, denoted as G-A-3 in Figure 1, has identical details to those of segment G-A-1. The vertical profiles of the second girder, denoted as G-C-1, G-E-2, and G-F-3 in Figure 1, had similar details.

Figure 2. Girder A prior to casting.

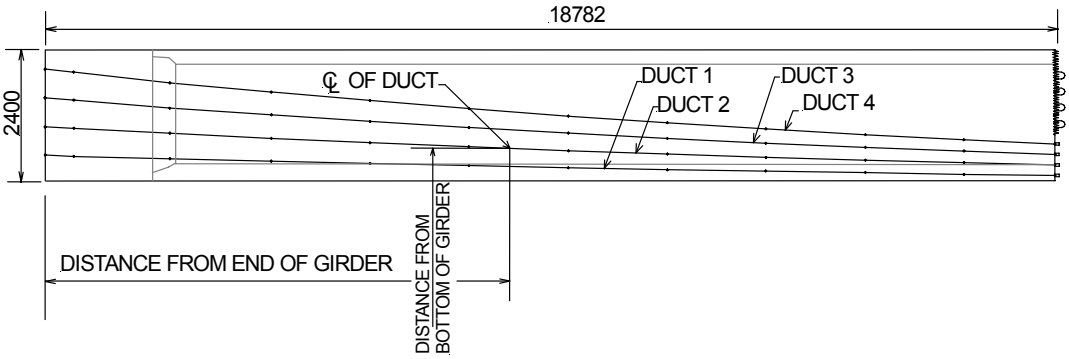

Figure 3. Vertical profile of girder segment G-A-1 (1 in. = 25.4 mm).

Table 1. Distance from bottom of Girder G-A-1 to bottom of duct at distance from end.

	Distance from End	0	500	2343	4187	6030	7873	9716	11560	13403	15246	17090	18782
DUCT 1	Distance from bottom of Girder	474	460	410	364	321	281	244	210	179	151	126	105
DUCT 2		1006	980	885	796	714	636	565	500	440	387	339	300
DUCT 3		1539	1500	1360	1229	1106	992	887	790	702	623	552	495
DUCT 4		2072	2020	1835	1661	1499	1348	1208	1081	964	859	766	690

Units in mm; (1 in. =25.4 mm)

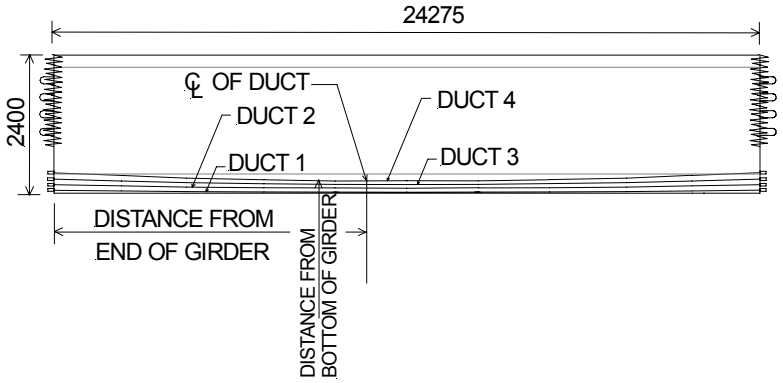

Figure 4. Vertical profile of girder segment G-A-2 (1 in. = 25.4 mm).

Table 2. Distance from bottom of Girder G-A-2 to bottom of duct at distance from end.

	Distance from End	0	2306	4764	7222	9679	12137	14595	17053	19510	21968	24275
DUCT 1	Distance from bottom of Girder	102	79	60	47	39	36	39	47	60	79	102
DUCT 2		294	250	214	188	172	167	172	188	214	250	294
DUCT 3		486	421	367	329	306	298	306	329	367	421	486
DUCT 4		677	592	521	470	439	429	439	470	521	592	677

Units in mm; (1 in. = 25.4 mm)

The post-tensioned modified bulb-tee section, W24PTMG, was used with an overall depth of 2400 mm (8 ft), as shown in Figure 5. The top and bottom flanges were 1290 mm (4 ft and 3 in.) and 1020 mm (3 ft and 4 in.) wide, respectively, and the web width was 200 mm (8 in.).

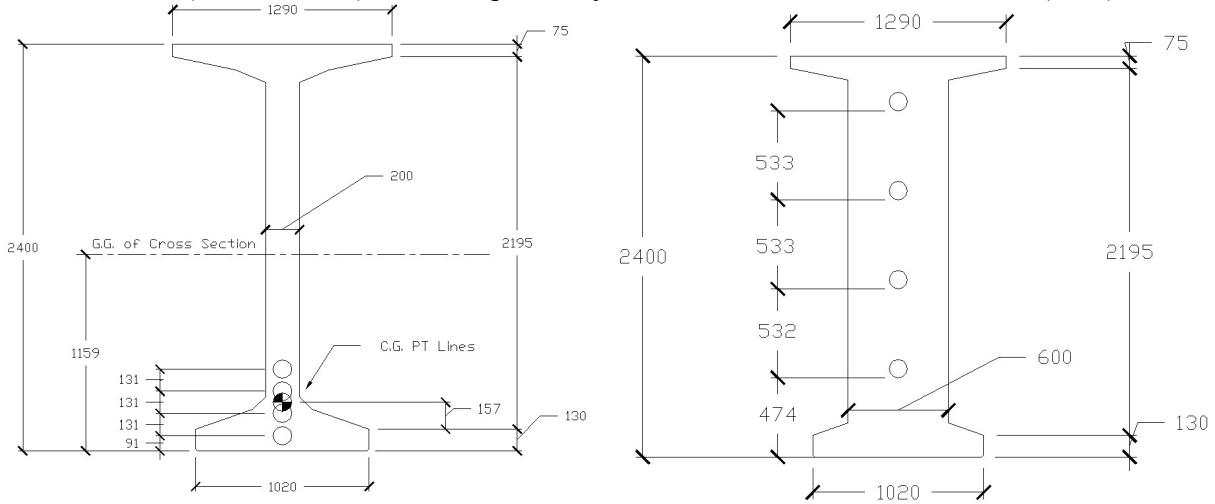

Figure 5. Girder cross-sections: (a) midspan, (b) anchors (1 in. = 25.4 mm).

Additional properties of the section at midspan, including the location of the post-tensioning ducts, are shown in Figure 5(a). The webs of the girders at the two anchorage zones were widened to accommodate the post tensioning anchorages, as shown in Figure 5(b). The material properties of the girders for design were: concrete compressive strength at release f'_{ci} = 38 MPa (5.5 ksi), and 28-day concrete compressive strength f'_c = 52 MPa (7.5 ksi). The measured

concrete compressive strength at 30 days was 63 MPa (9.1 ksi). Each girder had four tendons with 31 low relaxation, 12.7 mm (1/2 in.) diameter Grade 1860 MPa (270 ksi) strands per tendon that were housed in a metal galvanized duct.

Girder and Deck Installation

The construction of the 4500 South at I-15 overpass followed a four-stage erection procedure. The entire process, from placing the girders to opening the bridge for traffic, required 10 months to complete (from February to December 2000); Figure 6 shows the process. The first stage was to construct abutment seats at the north and south end of the bridge and erect temporary supports directly beneath the splice points. Second, the outer girder segments were erected and temporary bracing was placed between them. In the third stage, the middle girder segments were erected, the precast concrete deck panels were placed, and the splice diaphragms and deck were cast.

The deck was composed of precast concrete sections and a concrete topping surface. The precast concrete deck sections measured 2439 x 2439 mm (8 ft x 8 ft) and were 90 mm (3.5 in.) thick. The overall deck thickness was 215 mm (8-7/16 in.). The specified concrete strength of the splice diaphragm, cast-in-place deck, and precast panel concrete was 35 MPa (5 ksi). The bottom 1200 mm (4 ft) of the splice diaphragms was cast first; the remainder was cast with the cast-in-place deck. Figure 7 shows forming and placement of the splice diaphragms. After the splice diaphragms and deck had reached their specified strength, the tendons were passed through the ducts and post tensioned and the ducts were grouted. In the fourth and final stage, the abutment-end diaphragms were cast; at this time, the temporary supports and erection towers were removed and the parapets were cast on the deck. The erection towers were removed after post-tensioning; the span lifted off of the towers at the time of post tensioning.

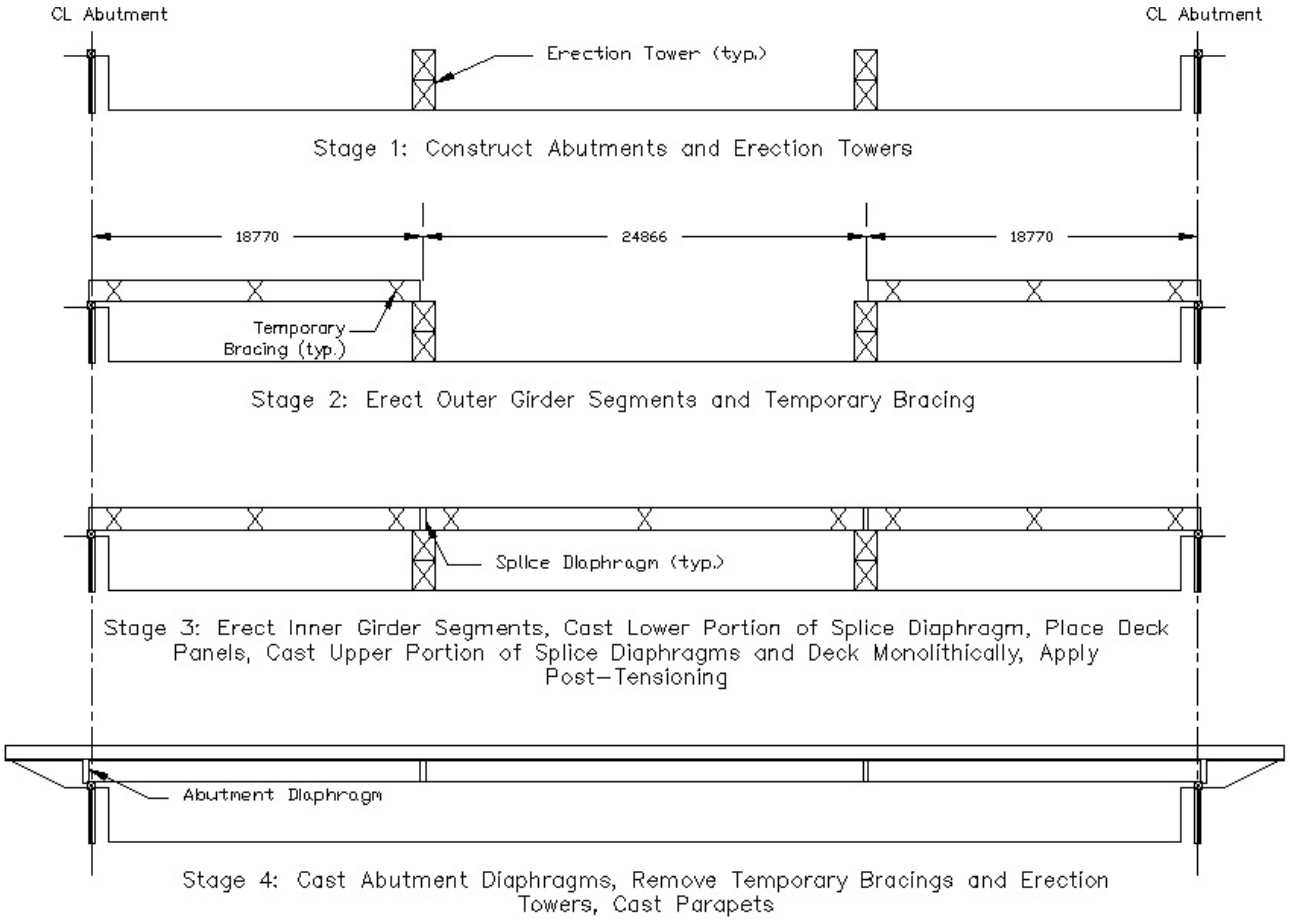

Figure 6. Spliced girder bridge erection sequence (1 in. = 25.4 mm).

Figure 7. Placement of splice diaphragms.

4. INSTRUMENTATION SETUP

The girders were instrumented with vibrating wire strain gauges in December 1999, prior to casting of the individual segments. At the time of post tensioning, the tendons of Girder A were instrumented with load cells to measure force in the tendons. After the bridge was completed, Girder A was instrumented with additional external vibrating wire strain gauges, tiltmeters, and temperature/humidity sensors; the parapet was also instrumented. Table 3 shows the timeline of construction and instrumentation of the 4500 South overpass from casting of the girder segments.

Vibrating Wire Strain Gauge (VWSG) Instrumentation

The internal and external gauges used to instrument the I-15 and 4500 South overpass girders were composed of a 152 mm (6 in.) metal tube with two 19 mm (3/4 in.) diameter endplates. As the tube undergoes strain between the endplates, the wire oscillates at different frequencies, which are then converted to strain. The gauges also give temperature readings, which allow the strain readings to be adjusted for temperature, for reference and calibration. It is necessary to adjust strain readings from internal gauges for temperature because the thermal coefficient of concrete is different than that of the gauge metal housing. The correction for strain is calculated based on the reference temperature of 22.8° C (73° F), by using the difference in the coefficients of thermal expansion of steel and concrete; after adjustment for temperature, the strain readings measure force induced strain, creep and shrinkage induced strain and strain associated with the stresses from restraint of thermal movement.

The first step in the instrumentation process was to obtain initial strain readings of the gauges for use as reference. The gauges were then attached to the non-prestressed steel of the girders in either a horizontal or vertical orientation (Figure 8). Figure 9 shows approximate locations of the strain gauges, as well as their orientations, for Girder A; the layup was similar for the other three segments denoted as G-C-1, G-E-2, and G-F-3 in Figure 1. Notation H indicates that the gauge measures horizontal strain in the concrete, along the girder axis; notation V indicates that the gauge measures vertical concrete strain along the web axis. The vertical gauges were placed to detect any difference in the readings on two sides of the splice. Girder A was also instrumented with externally mounted vibrating wire strain gauges that perform similar to internal gauges. The only difference is the fact that external gauges are mounted to the concrete surface. Gauges 22 through 31 of Girder A, segments G-A-2 and G-A-3, are external gauges, while all other gauges are internal. The external gauge readings were not compared to internal gauge readings but were monitored to show any changes with time.

Load Cell Installation

The eight load cells used in this study were custom manufactured by the Construction Technology Laboratories (CTL), Inc., and were installed at the north and south ends of Girder A at the time the tendons were jacked on April 27 and 28, 2000. The load cells measured 330 mm (13 in.) tall, 235 mm (9 ¼ in.) outer diameter, and 178 mm (7 in.) inner diameter. The load cells were numbered LC1 to LC4 from top to bottom on the north end of the girder (jacking end) and LC5 to LC8 on the south end (anchored end). Figure 10 shows the installed load cells LC1 to LC4 on the north end of Girder A just after post-tensioning on April 28, 2000. The load cells were rated at a force of 4450 kN (1000 kips) each. As shown in Figure 10, the bearing caps, which are normally flush with the girder face, were placed on the outside of the load cell and the strands were fixed at that point. The load cells were sealed and isolated from the concrete of the abutment diaphragms by encasing them in specially constructed tubes.

Table 3. Sequence of events.

DATE	EVENT
12/13/99	Strain Gauge Placement Girder A
12/13/99	First Readings Taken Girder A
12/15/99	Cast Girder A
12/18/99	First Readings Taken of Cast Girder A
12/18/99	Strain Gauge Placement Girder Segments G-C-1, G-E-2, G-F-3
12/18/99	First Readings Taken Girder Segments G-C-1, G-E-2, G-F-3
12/20/99	Cast Girder Segments G-C-1, G-E-2, G-F-3
12/20/99	First Readings Taken of Cast Girder Segments G-C-1, G-E-2, G-F-
02/09/00	Girders Taken to Site and Set in Place
03/08/00	Splice Diaphragm placement
04/17/00 - 04/18/00	Deck Placement
04/27/00	P/T Tendons 1 thru 12 (LC[+] 1,2,5,6 of Study Girder Included)
04/28/00	P/T Tendons 13 thru 25 (LC 3,4,7,8 of Study Girder Included)
04/27/00 - 04/28/00	Load Cells Placed and First Readings Taken
05/01/00	P/T Tendons 26 thru 32
05/04/00	Grout tendons
05/23/00	South End Diaphragm placement
06/03/00	North end Diaphragm placement
06/23/00	North and South Approach Slab Placement
06/29/00	First Deck Survey Readings Taken
07/28/00	East Bridge Barrier (Parapet) Placement
08/22/00	Initial Parapet Readings Taken
11/07/00	West Bridge Barrier Placement
11/09/00	West Approach Slab Barrier Placement
12/17/00	Bridge Opened to Traffic
11/10/02	External Vibrating Wire Strain Gauges Installed
11/10/02	Tiltmeters Installed at North Splice
1/04/03	Data Collection System Installed

[+]LC = load cell

(a) (b)

Figure 8. Internal Vibrating Wire Strain Gauge placement: (a) horizontal and (b) vertical.

Tiltmeter Installation

Four tiltmeters were installed on Girder A. A biaxial mounting bracket was used which allowed the tiltmeters to be mounted at right angles to each other, enabling in-plane and out-of-plane measurements. Figure 9 shows the locations of the tiltmeters on Girder A. Tiltmeter 1 was located on the south side of the north splice diaphragm in girder segment G-A-2, whereas Tiltmeter 3 was located on the north side of the same diaphragm in girder segment G-A-3 (to measure any differential rotation occurring at the splice in the plane of the girder). Tiltmeter 4 was located at the midspan of girder segment G-A-3. Tiltmeter 2 was installed in girder segment G-A-3 to measure rotation in the plane of the diaphragm, at 90 degrees to the plane of the girder.

Data Collection System

At the beginning of the study, readings were taken manually. Once all bridge elements were completed, a data collection system was installed using wireless data transmission. This system allowed data to be collected every 15 minutes, as opposed to monthly, greatly enhancing the database and showing the effects of temperature changes throughout a given day. The data collection system consisted of two dataloggers and eight multiplexers. Each multiplexer contains only one type of sensor (vibrating wire strain gauge, load cell, etc.). The readings taken by the dataloggers were stored in an internal memory. Dataloggers on both ends of the bridge were connected to a common hub that was linked to a wireless data transmitter/receiver, which was aligned to another transmitter/receiver at a recording station at the University of Utah campus. Data were downloaded from the bridge to the recording station through a wireless connection. The collection rate for the dataloggers was every five minutes, with the average of three readings recorded every 15 minutes in downloadable memory.

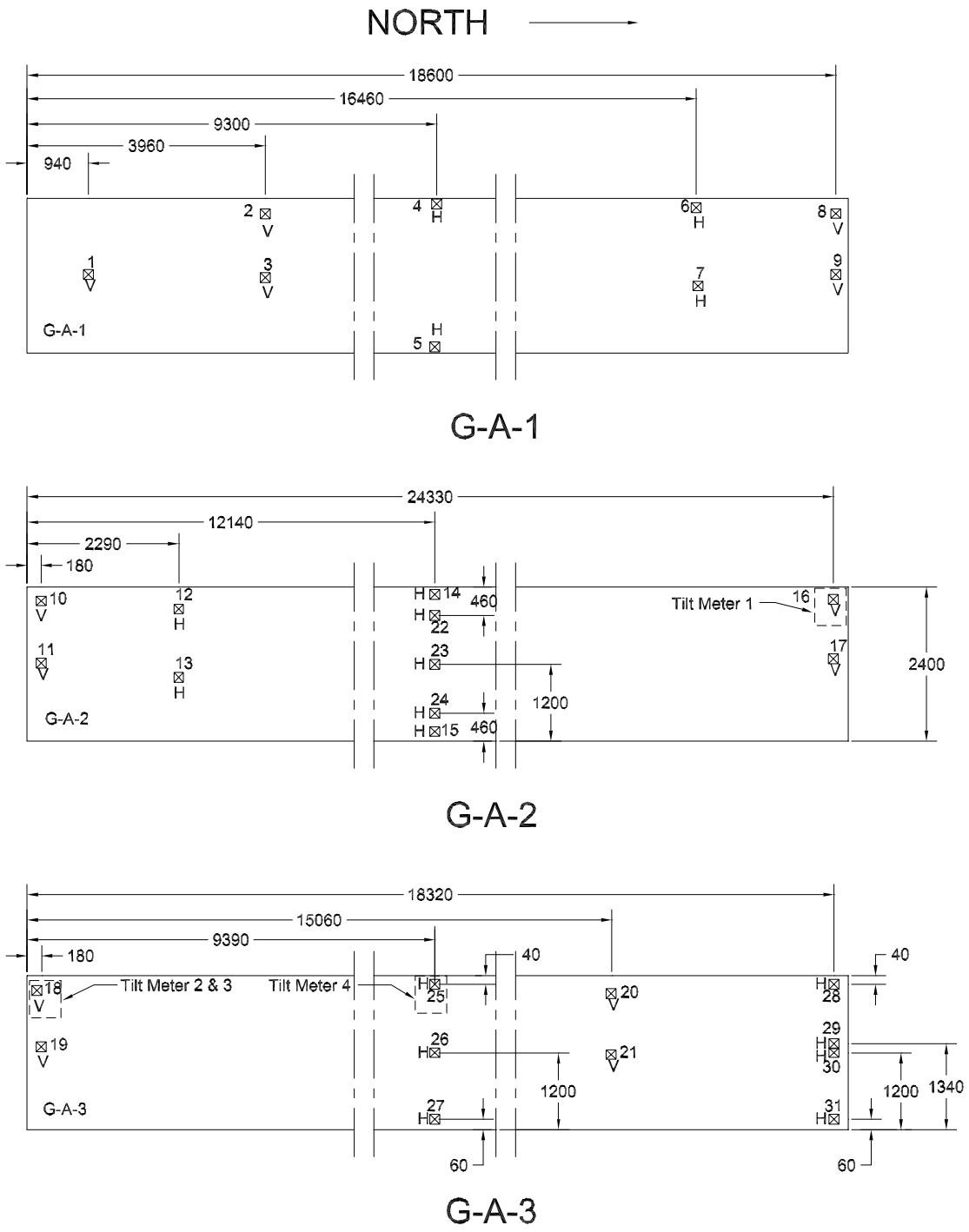

Figure 9. Vibrating wire strain gauge locations – Girder A elevation: V=vertical vibrating wire strain gauge; H=Horizontal vibrating wire strain gauge (1 in. = 25.4 mm).

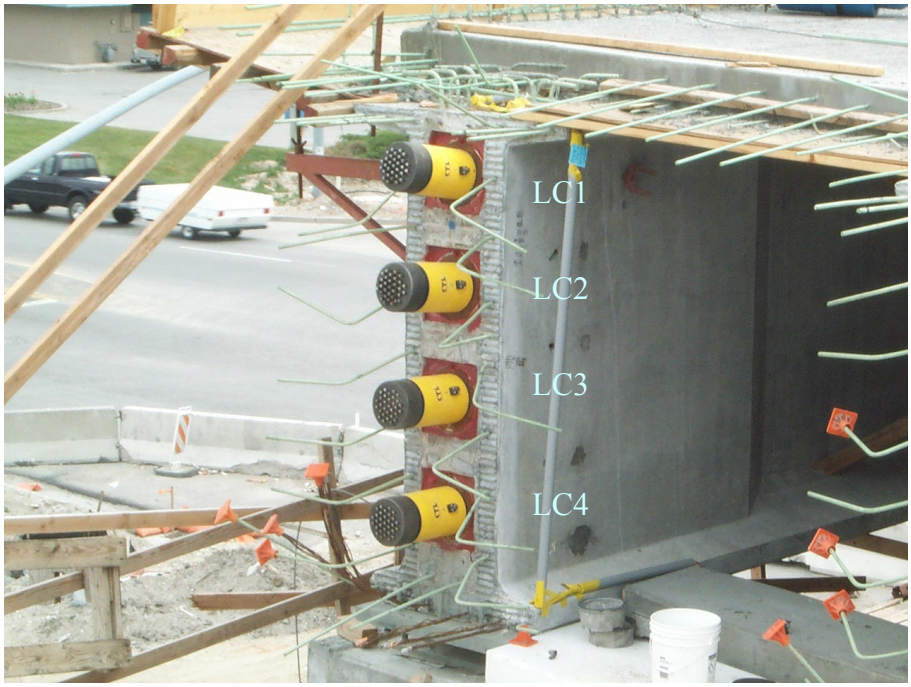

Figure 10. Load cells 1-4 installed on the North End of Girder A.

5. EXPERIMENTAL OBSERVATIONS

Post Tensioned Tendon Losses

Measurements from Girder A and the three segments denoted as G-C-1, G-E-2, and G-F-3 in Figure 1, began on December 18, 1999. Losses for various dates throughout the study period averaged for all load cells are shown in Table 4. As shown in Table 3, load cells LC1, LC2, LC5, and LC6 were stressed on April 27, 2000, while load cells LC 3, LC 4, LC 7, and LC 8 were stressed the next day. Thus, in Table 4, the first loss percentages are shown for the first reading after the initial reading; the values shown do not include the initial anchorage seating and friction loss. It is evident from Table 4 that the initial losses after a one-day period are between 1.1% and 3.4%. The initial reading of each load cell was taken immediately after anchorage was completed. The initial anchorage seating and friction loss was recorded independently as 222 kN (50 kips) per tendon or an average loss of 5.5%. Therefore, the total losses including the anchorage seating loss, friction loss, and elastic shortening, amount to between 6.6% and 8.9% at the abutments.

The tendons were grouted on May 4, 2000. Figure 11 shows load cell data covering the initial 63 days after jacking, from April 27, 2000 through June 29, 2000, and Figure 12 shows the entire study period. In early June 2000, approximately two weeks after placement of the south-end abutment, load cell LC8 began to show erratic readings as shown in Figure 11; shortly after October 2001, load cell LC4 also began to show erratic readings, as shown in Figure 12. As can be seen in Figures 11 and 12, there are various periods when load cell data is missing, when the instruments were inaccessible. Figure 11 shows that placement of the south-end abutment diaphragm caused little or no increase in stresses in the load cells; this is because Girder A was free to re-adjust to the imposed restraint at the south-end abutment by free movement and rotation at the north-end abutment. Placement of the north-end abutment diaphragm on June 3, 2000 caused a stress increase in all four load cells at the north end compared to May 23, 2000, as indicated by the measurements of load cells LC1-LC4 in Figure 11. The abutments are considered to be semi-integral; the difference in tendon reaction between the placement of the north and south end-abutment diaphragms is likely due to the fixity from the south end (which had already been placed) combined with the weight of the abutment mass and its subsequent

Table 4. Tendon prestress losses from load cells (%).

Load Cell	1	2	3	4	5	6	7	8	Days	Years
4/27/2000 15:50	0.6%				0.7%				0	0.00
4/28/2000 14:00	2.2%	2.0%			2.8%	0.8%			1	0.00
4/28/2000 14:37	3.0%	3.0%	0.9%		3.9%	1.9%	1.3%		1	0.00
5/6/2000 0:00	5.8%	5.5%	3.5%	2.6%	7.2%	4.8%	4.8%	3.7%	8	0.02
5/23/2000	6.3%	6.3%	4.6%	3.6%	8.2%	6.2%	5.4%	4.6%	25	0.07
6/3/2000	6.3%	6.0%	4.3%	3.5%	8.7%	6.9%	7.0%	5.7%	36	0.10
6/29/2000	8.9%	8.7%	7.1%	5.7%	*	*	*	*	62	0.17
9/5/2000	10.1%	9.5%	7.7%	6.3%	*	*	*	*	130	0.36
10/12/2001	13.4%	11.8%	10.0%	7.8%	12.6%	10.3%	10.4%	37.4%	532	1.46
10/6/2002	14.9%	12.9%	11.1%	30.3%	13.3%	11.2%	11.9%	45.4%	891	2.44
12/31/2003	16.5%	13.8%	14.4%	39.6%	14.8%	12.9%	12.6%	58.4%	1342	3.68

* = Measurement not available

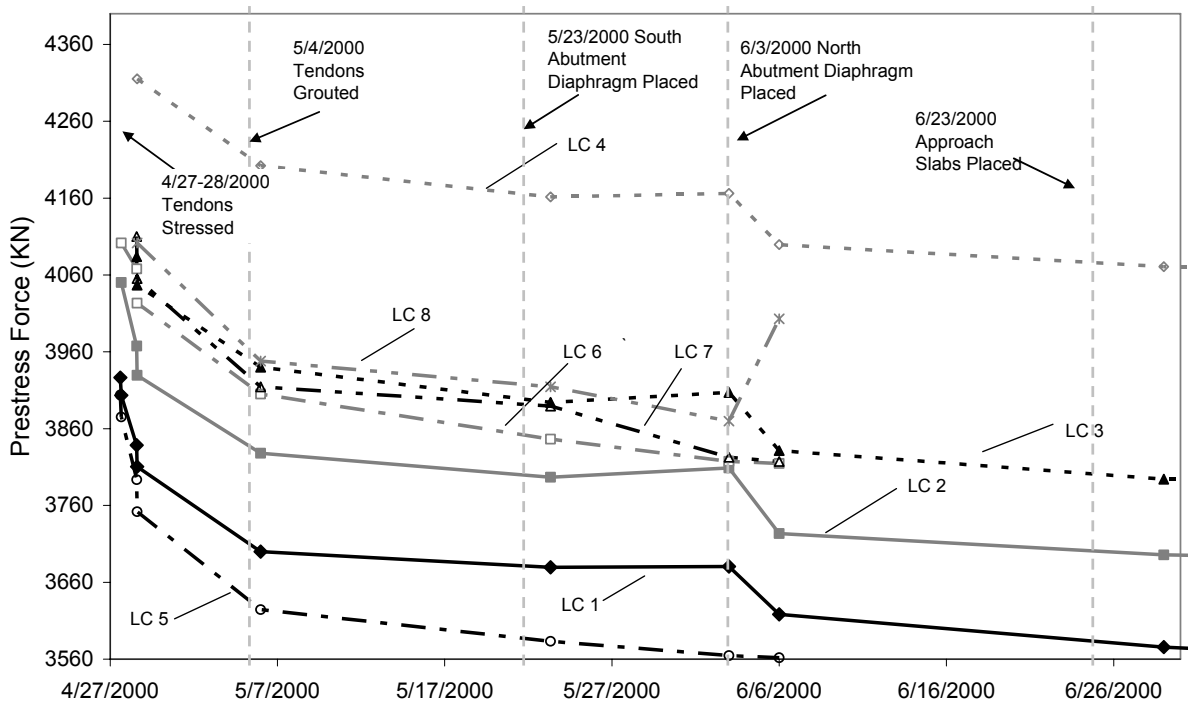

Figure 11. Effective prestress force after losses vs. time: load cell readings for initial 63 days - Tendon 1, top: (LC1 & LC5); Tendon 2: (LC2 & LC6); Tendon 3: (LC3 & LC7); Tendon 4, bottom: (LC4 & LC 8); (1 kip = 4.448 kN).

settlement. The stresses in the tendons due to this effect stabilized at this time, after which all tendons started displaying time-dependent losses, as shown in Figure 12.

From Figure 12 and Table 4, the top three tendons reached equilibrium after December 2002 (980 days) and have maintained a constant force. The top three tendons have experienced time-dependent losses after 1342 days ranging from 12.6% to 16.5%, with the top tendon having the largest loss, as shown in Table 4. It should be stressed that after May 4, 2000, when the four tendons were grouted, the load cells are measuring losses due to creep only at the anchorage zones. After May 4, 2000, the tendon forces and losses were calculated at midspan based on vibrating wire strain gauge readings from gauge G14 at the top and gauge G15 at the bottom of the girder, as shown in a later section.

Strains in the Concrete of Instrumented Girders

Strain readings in the concrete, as recorded by the vibrating wire strain gauges, were taken twice per week in the last two weeks of December 1999 through the beginning week of February 2000. Readings were then taken on a weekly basis until the deck was placed in April 2000. Readings were then taken on a monthly basis, with some exceptions when the gauges were not accessible, until the data acquisition system was installed in January 2003. After this time, readings were taken every five minutes and an average of three readings was recorded every 15 minutes.

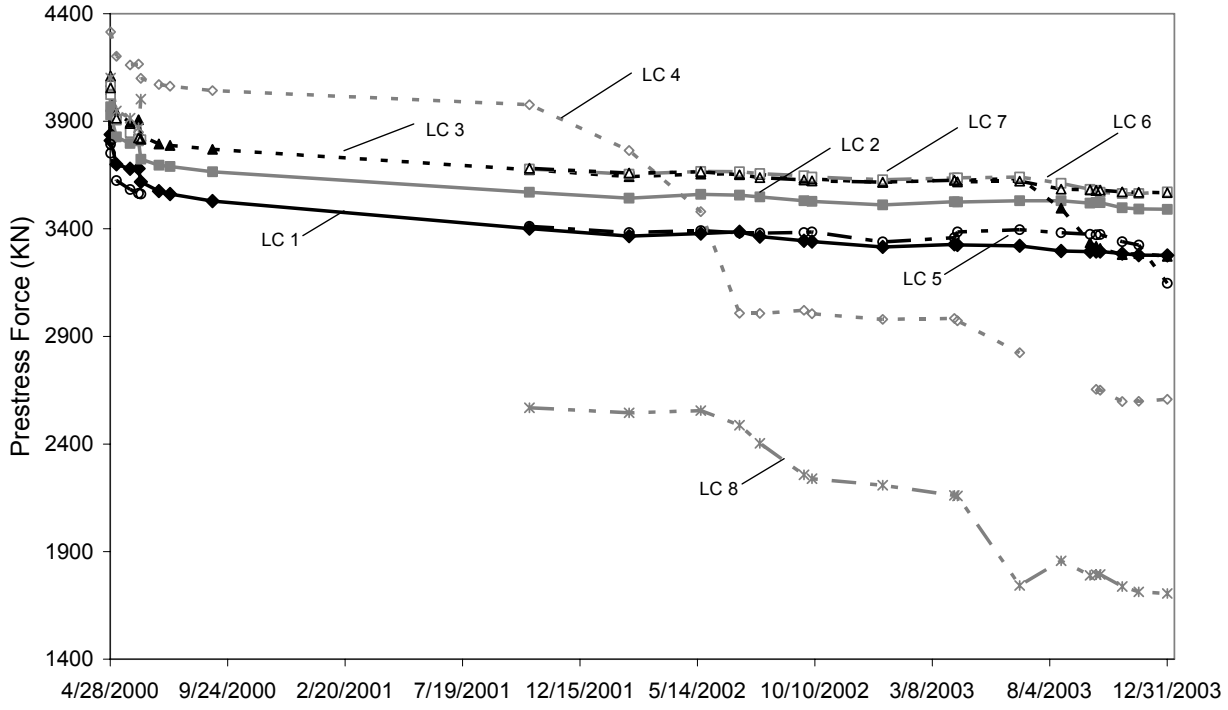

Figure 12. Effective prestress force after losses vs. time: load cell readings from April 27, 2000 to December 31, 2003 - Tendon 1, top: (LC1 & LC5); Tendon 2: (LC2 & LC6); Tendon 3: (LC3& LC7); Tendon 4, bottom: (LC4 & LC 8); (1 kip = 4.448 kN).

Vertical VWSG

Vertical gauges were installed to measure differential strains in the concrete perpendicular to the girder axis in the plane of the girder web, as identified in Figure 9. Figure 13 shows the uniformity of strains throughout the span of Girder A. As shown in Figure 13, the gauges just to the south (G16 and G17) and north (G18 and G19) of the north splice of Girder A, have readings that are more closely grouped than the corresponding gauges for segments G-E-2 and G-F-3. This is expected because segments G-E-2 and G-F-3 were placed on Girders E and F and therefore do not share a common splice connection. This indicates that the splices are performing well in their task of maintaining continuity between the precast concrete girder segments. The uniformity and consistency among the girders, shown in Figure 13, indicates satisfactory diaphragm performance and lack of differential strain (deflection) at the splices.

At the time of post-tensioning, April 27-28, 2000, nearly all gauges experienced a drop up to 300 microstrains, indicating an increase in tensile strain (or a decrease in net compressive strain) related to end zone bursting/cracking moment. In Figure 1.13, VWSG G16 and G18, which were in the girder top flange on opposite sides of the north splice from one another, show a much larger negative strain reading than VWSG G17 and G19, which were located directly below them at mid-height of the girder segments; G16 and G18 drop well below their initial values, indicating that tensile stresses occur near the top fiber, while G17 and G19 remain above their initial values, indicating considerably lower compressive stresses at these locations. However,

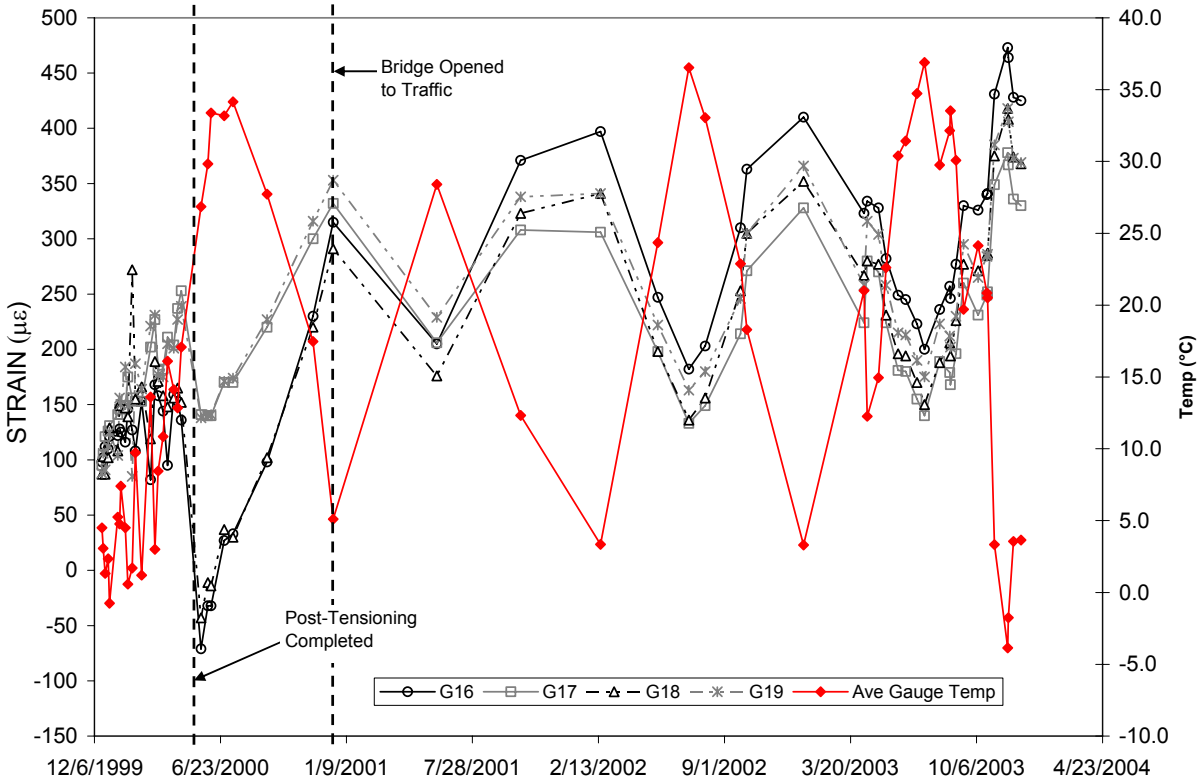

Figure 13. Temperature compensated vertical strain gauge readings at north splice of Girder A (+ = compression).

the tensile strains in Figure 13 are very small, less than 75 microstrain. These effects are reversed in the period after placement of the end-abutment diaphragms, which took place on May 23, 2000 for the south-end and June 03, 2000 for the north-end abutment diaphragm.

On December 17, 2000 the northbound overpass was opened to traffic. All gauges near the top fiber and at mid-height of the girder section show compressive strains at this time, as shown in Figure 13; a small difference occurred between readings at similar locations on opposite sides of the splice points. In Figure 13, G16 and G18, which are at the top flange on opposite sides of the north splice point, gave a differential reading of 30 microstrain in compression on Dec. 17, 2000. This behavior was also seen from G8 and G10, placed at similar locations at the south splice point, with a differential reading of 50 microstrain in compression. In both cases, the compressive strains at the top flange were greater for gauges closer to midspan (G16 and G10) than for gauges on the outer side of the two splice points, closer to the abutments (G18 and G8). The gauges at mid-height of the section experienced the opposite effect. The gauges inside segment G-A-2 (G17 and G11) had smaller compressive strains than the gauges located on the outer side of the two splice points (G19 in G-A-3 and G9 in G-A-1). These gauges were located below the neutral axis of the girder/slab unit and therefore experienced the opposite strain.

Horizontal VWSG

The purpose of the horizontally oriented gauges was to measure compression and tensile strains in the concrete in a direction parallel to the axis of the girder; consequently most of these

gauges were placed in the top and bottom flanges of the girder. Inspection of the gauge readings in Figure 14 shows that, just prior to post-tensioning (April 27-28, 2000), G4 and G14, located in the top flange of Girder A in the south segment (G-A-1) and middle segment (G-A-2) in Figure 9, show compressive strains of 346 and 394 microstrain, respectively, which are larger than their counterparts in the bottom flange, G5 and G15 at 235 and 204 microstrain, respectively. This is consistent with the behavior of a simply supported beam under gravity loads. The three girder segments were placed on temporary supports during erection; they had been cast with pretensioned and non-prestressed steel reinforcement for dead load moment during transportation and erection; therefore they never experience tensile stresses in any of the readings during erection, as can be seen in Figure 14. It is seen that the compressive strain from gauge G14 (394 microstrain) is larger at the top of the girder in the middle segment, than in the third span from G4 (346 microstrain). For strains in the bottom flange, the middle segment gauge G15 (235 microstrain), shows a smaller net compressive strain than the third segment gauge G5 (204 microstrain). After post-tensioning, (April 27-28, 2000), all gauges indicate a large jump in compressive strain; from the larger bottom flange strain gauge readings in Figure 14, it is clear that Girder A is deflecting upwards. Gauges G4 and G14 in the top flange, now report compressive strains after post-tensioning of 879 and 898 microstrains, respectively; gauges G5 and G15 in the bottom flange now report the largest compressive strains at 1112 and 973 microstrains, respectively. Gauge G15 in the bottom flange at midspan reports a smaller compressive strain than the gauge in the bottom flange of the third segment, G5, mainly due to the self-weight stresses of the girder, deck, and parapet, inducing a larger strain effect at midspan, which counters the compressive strain. This behavior is similar for the other three girder segments G-C-1, G-E-2, and G-F-3.

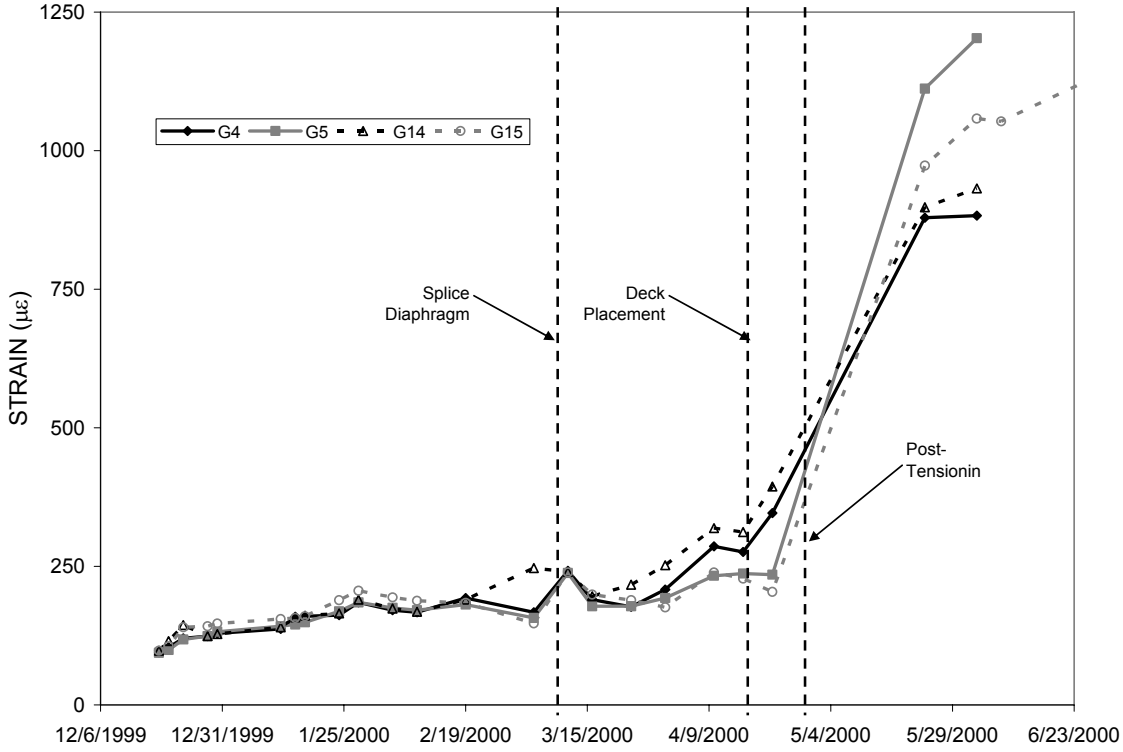

Figure 14. Temperature compensated readings of selected horizontal strain gauges during initial days for Girder A (+ = compression).

The increase in compressive strain as a result of creep and shrinkage discussed previously continued until December 17, 2000 when the bridge was opened to traffic, as seen from gauge G15 in Figure 15. This behavior was also observed in vertical strain gauges, as shown in Figure 13. Concrete strains after this time have come to equilibrium and only seasonal temperature-related strains are noted after this point. This eight-month period of compressive strain increase, from April to December 2000, required to reach equilibrium is due to creep and shrinkage of concrete. As the tendons were stressed they created large compressive strains in the girders; these compressive strains were recorded by the VWSGs as discussed previously and resulted in the strain increases seen in Figure 14. After this initial strain increase, the concrete continued to creep as the force on the section was maintained, resulting in the additional strain increases seen in Figure 15 and recorded by G15. Other gauges in Figure 15 were not accessible during this period due to construction, but these gauges became available again in December 2000 when the bridge was opened to traffic, and they show similar behavior to that of G15. This observation is confirmed by examination of creep and shrinkage strains in the creep and shrinkage concrete cylinder tests, which show that strains have largely come to equilibrium after 8 months. Figure 16 shows the tendon forces measured from horizontal VWSGs G14 at the top and G15 at the bottom of the girder section at midspan. After 1.5 years, on Oct. 12, 2001, 93% of the losses have taken place; comparing the readings from VWSG's in Figure 16 and load cell readings in Figure 11, the losses at midspan are less than the losses at the ends. After approximately four years the average losses at midspan are 14.5% based on the horizontal VWSG readings.

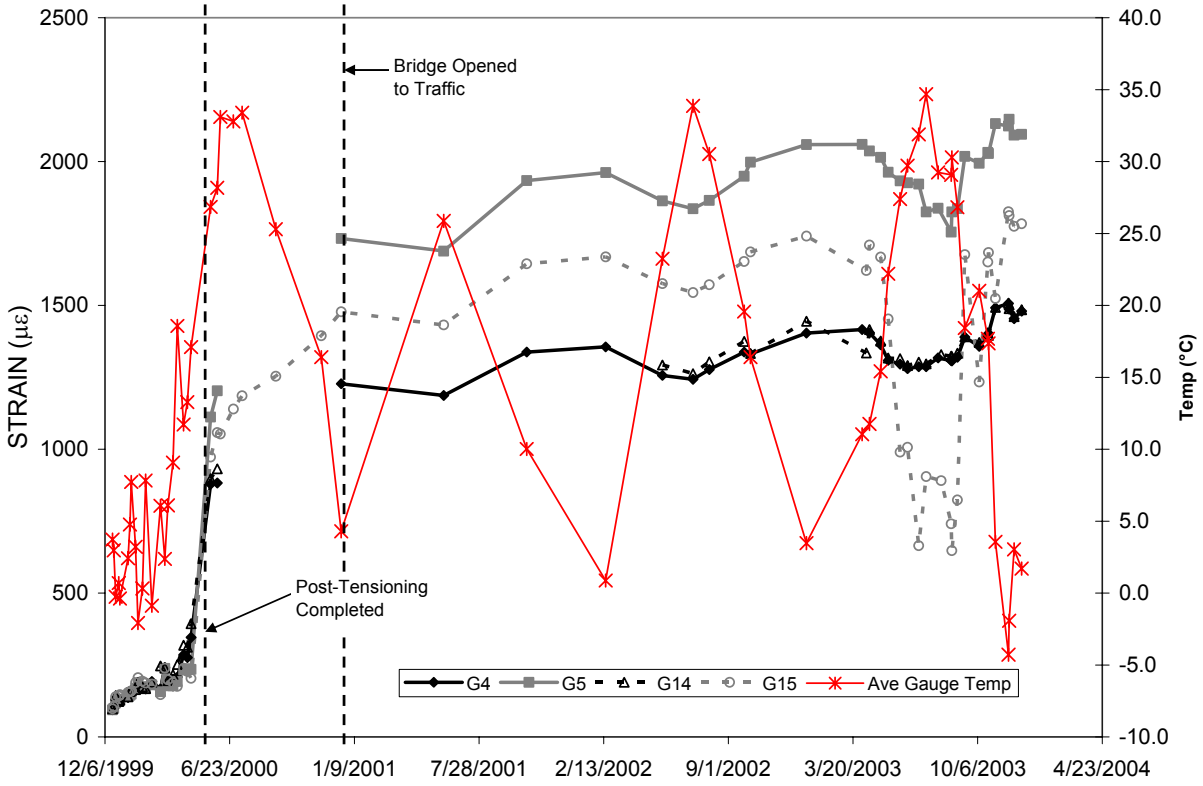

Figure 15. Temperature compensated strain gauge readings of selected horizontal gauges in Girder A (+ = compression).

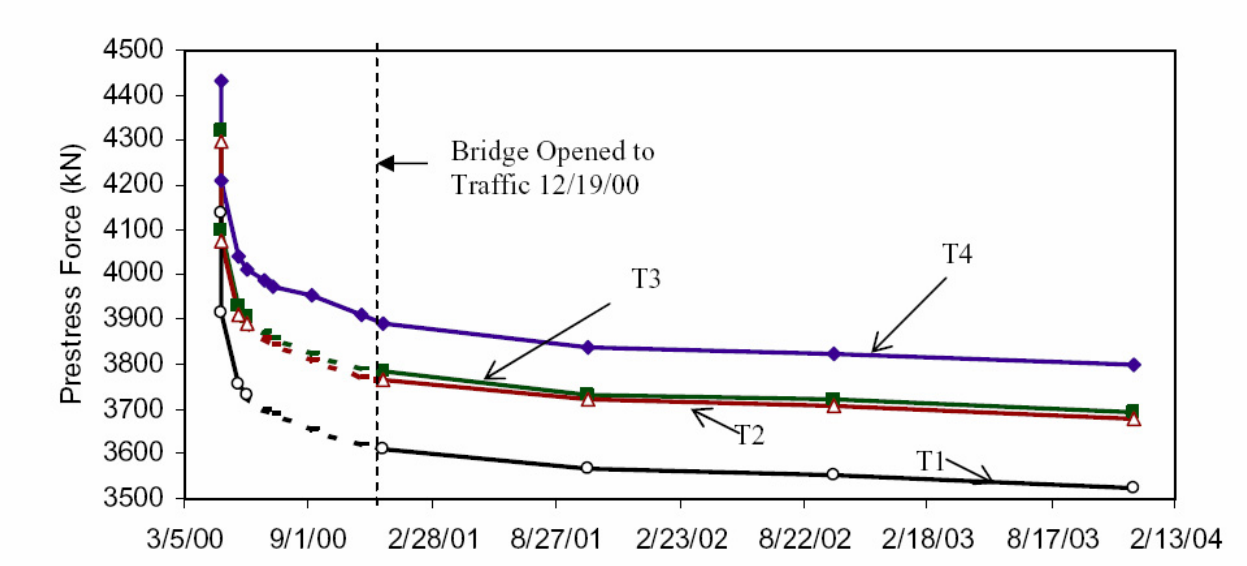

Figure 16. Effective prestress force after losses from vibrating wire strain gauges at midspan vs. time: Tendon T1, top; Tendon T4, bottom; (1 kip = 4.448 kN).

6. CONCRETE MODULUS OF ELASTICITY, CREEP, AND SHRINKAGE

Creep and shrinkage tests were performed to evaluate the ultimate creep coefficient and ultimate shrinkage strain. Additionally, the tests produced concrete compressive strength and modulus of elasticity properties at various ages of curing. Concrete compressive strength and modulus of elasticity, creep, and shrinkage tests were performed on cylinders made from the same concrete used to cast the post-tensioned precast concrete spliced girders. The cylinders were cast on December 15, 1999.

Concrete Modulus of Elasticity

Concrete compressive strength was determined according to ASTM C 39 (ASTM 1999) and modulus of elasticity according to ASTM C 469 (ASTM 1994) by the Construction Technology Laboratories (CTL), Inc. Tests were performed on 152 x 305 mm (6 x 12 in.) cylinders for 3-day, 30-day, and 90-day old concrete. The compressive strength increased from 44 MPa (6.4 ksi) for 3 day old concrete to 82 MPa (11.9 ksi) for 90-day old concrete, as shown in Table 1.5. The equation recommended by ACI-318 (ACI 2005) and AASHTO (AASHTO 2004) to determine modulus of elasticity E_c, from specified concrete compressive strength f'_c, and unit weight w_c, is given as:

$$E_c = 0.043 w_c^{1.5} \sqrt{f'_c} \text{ (MPa)}; \quad E_c = 33 w_c^{1.5} \sqrt{f'_c} \text{ (psi)} \tag{1}$$

ACI Committee 363 (ACI 1997) suggested that Eq. (1) overestimates modulus of elasticity for concrete with compressive strength above 41 MPa (6 ksi). The committee recommended the following equation to determine modulus of elasticity:

$$E_c = \left(3.32\sqrt{f'_c} + 6895\right)\left(\frac{w_c}{2320}\right)^{1.5} \text{(MPa)}; \quad E_c = \left(40000\sqrt{f'_c} + 10^6\right)\left(\frac{w_c}{145}\right)^{1.5} \text{(psi)} \tag{2}$$

Using Eq. (1) and (2) and assuming w_c = 2323 kg/m^3 (145 lb/ft^3), the predicted moduli of elasticity are found as shown in Table 5. Equations (1) and (2) overestimate the true elastic modulus of the 3-day, 30-day, and 90-day old concrete. However, Eq. (2) suggested by ACI Committee 363 is much closer to the experimental results and should be used to predict the concrete modulus of elasticity.

Table 5. Modulus of elasticity at different ages and comparison with ACI 318 and ACI 363.

Concrete Age	f'_c Measured (MPa)	E_c Measured (MPa)	E_c ACI 318 (MPa)	E_c ACI 363 (MPa)	(E_c ACI 318) versus (Ec Measured)	(E_c ACI 363) versus (Ec Measured)
3-Day	44	26550	31760	28950	+19.6%	+9.0%
30-Day	63	28480	37920	33220	+33.2%	+16.7%
90-Day	82	34410	43230	36910	+25.7%	+7.3%

Ultimate Creep Coefficient

Creep and shrinkage tests were performed as per ASTM C512 (ASTM 1994) by CTL, Inc. Tests were performed on 152 x 305 mm (6 x 12 in.) cylinders with an applied unit stress of approximately 40% of the concrete compressive strength. Humidity levels of 50% were used for both the preload environment and the loaded environment and temperature was maintained at 23.0° ± 1.7° C (73.4° ± 3.0° F). The creep and shrinkage test for the 3-day old concrete cylinders began on December 18, 1999 and continued for 895 days until May 31, 2002. For all tests, two cylinders were tested for creep and two were tested for shrinkage. Results for the 3-day old concrete creep and shrinkage test are shown in Figure 17 and 18, respectively. At the time of the 3-day test, the cylinders had a compressive strength of 44 MPa (6.4 ksi).

Table 6 contains the value of v_u, the ultimate creep coefficient, which best satisfies the equation:

$$v_t = \frac{(t - t_i)^{0.6}}{10 + (t - t_i)^{0.6}} \cdot v_u \tag{3}$$

where v_t = creep at time t. Equation (3) is a basic model used to predict creep as given by Branson and Kripanarayanan (1971) and ACI Committee 209 (ACI 1997); $(t\text{-}t_i)$ represents the number of days elapsed since the loading of the concrete began.

The best fit value of v_u (measured) in Table 6 and used in Figure 17, has been chosen in the following manner: First, a value of v_u was estimated; using this initial trial of v_u, the sum of the squared deviations between the measured and predicted value of v_u was calculated; next, a range of values around the initial predicted value were tried and the sum of the squared deviations were calculated and recorded for each trial value. An absolute minimum or "best fit" for v_u was found by plotting the trial values versus the results and finding the point of zero slope.

The value shown in the column labeled "ACI 209" in Table 6 was determined using the adjustment factors found in the report by ACI Committee 209 (ACI 1997). The values used to compute the correction factors for creep and shrinkage are shown in Table 6. Adjustments were made for loading age γ_{la}, relative humidity γ_λ, and minimum thickness using the volume-surface ratio method γ_{VS}. Figure 17 shows a plot of measured versus predicted ultimate creep coefficient using the values of v_u shown in Table 6 for the 3-day old concrete, for the "best fit", and the ACI 209 methods, respectively. At eight months, the creep coefficient had reached 87% of its ultimate value. Based on the tests performed from the concrete used in this bridge, the recommended value of the ultimate creep coefficient is 2.16; from the ACI 209 method, a value of 2.56 is obtained for the ultimate creep coefficient.

Ultimate Shrinkage Strain

Table 6 shows the value of the ultimate shrinkage strain $(\varepsilon_{sh})_u$ that satisfies the equation:

$$(\varepsilon_{sh})_t = \frac{(t - t_i)}{55 + (t - t_i)} (\varepsilon_{sh})_u \tag{4}$$

where $(\varepsilon_{sh})_t$ = shrinkage strain at time t. Equation (4) was recommended by Branson and Kripanarayanan (1971) and ACI Committee 209 (1997). The base value for $(\varepsilon_{sh})_u$ of 780×10^{-6} has been adjusted for humidity, and minimum thickness as described for creep in Eq. (3), with the values shown in Table 6.

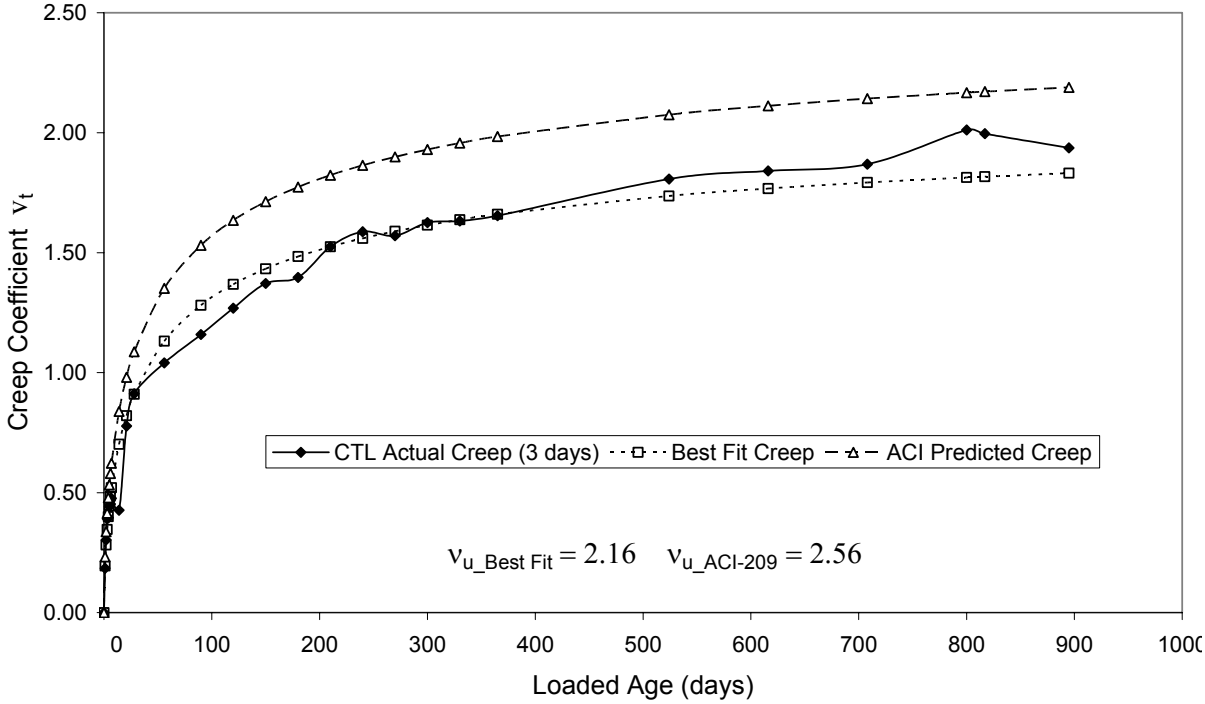

Figure 17. Actual vs. theoretical creep at concrete age of 3 days.

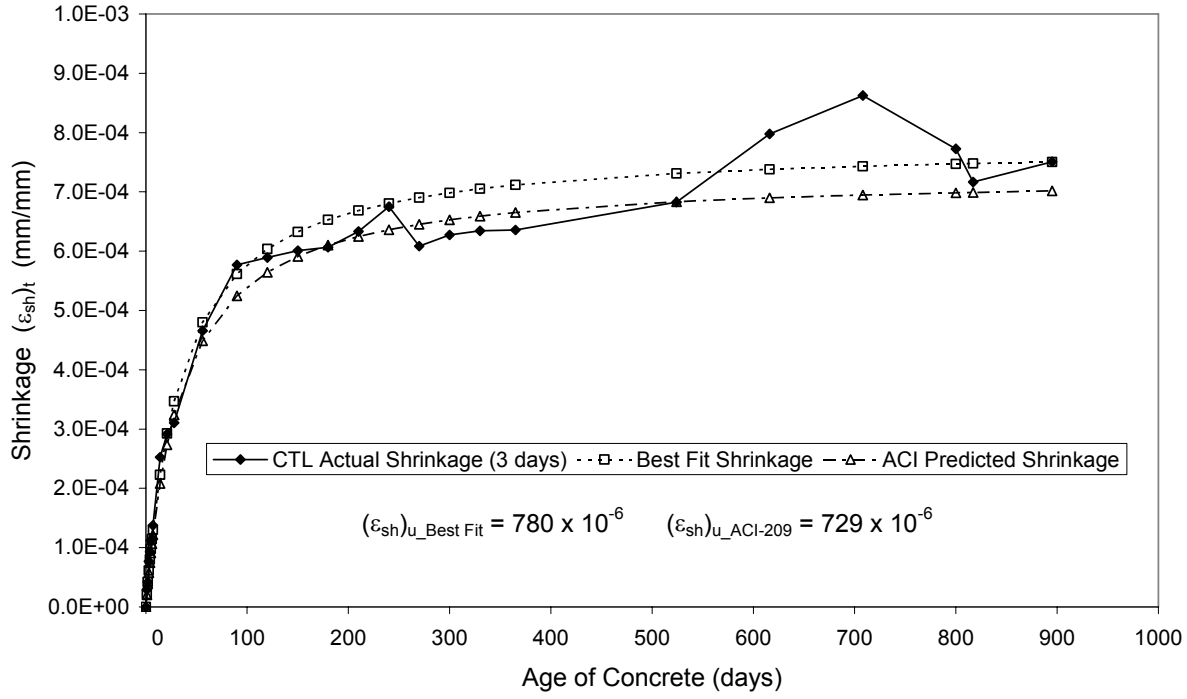

Figure 18. Actual vs. theoretical shrinkage strain at concrete age of 3 days.

Table 6. Ultimate values from CTL creep and shrinkage tests and comparison to ACI 209.

	Ultimate Creep Coefficient, v_u		Ultimate Shrinkage Coefficient, $(\varepsilon_{sh})_u$	
	Best Fit	ACI 209	Best Fit	ACI 209
	2.16	2.56	780×10^{-6}	729×10^{-6}
Loading Age Component, γ_{la}	-	1.098	-	-
Humidity Component, γ_{λ}	-	0.935	-	0.900
Volume/Surface Component, γ_{VS}	-	1.061	-	1.039
Creep Correction Factor, γ_c	-	1.089	-	-
Shrinkage Correction Factor, γ_{sh}	-	-	-	0.935

Notes for ACI 209 method: 1. $v_u = (2.35)\gamma_c$; $(\varepsilon_{sh})_u = (780x10^{-6})\gamma_{sh}$

2. $\gamma_c = (\gamma_{la})(\gamma_{\lambda})(\gamma_{VS})$; $\gamma_{sh} = (\gamma_{\lambda})(\gamma_{VS})$

A best-fit value of $(\varepsilon_{sh})_u$ is shown in Table 6 using the most appropriate value found as described previously for the creep coefficient. The plot for shrinkage strain is given in Figure 18, using the experiments, the best-fit value, and the ACI-209 (ACI 1997) determined value of $(\varepsilon_{sh})_u$, corrected using the correction factors from Table 6. At eight months, the shrinkage strain had reached 92% of its ultimate value. Based on the tests performed from concrete used in this bridge, the recommended value of the ultimate shrinkage strain is 780×10^{-6}; from the ACI 209[20] method, a value of 729×10^{-6} is obtained for the ultimate shrinkage strain.

7. POST-TENSIONED SPLICED GIRDER LOSS PREDICTIONS

Lump sum losses in prestressed concrete construction were recommended by the American Concrete Institute (ACI) and American Society of Civil Engineers (ASCE) Joint Committee 323 (1958) for routine design purposes as early as 1958. For post-tensioned members, the lump sum losses were recommended as 172 MPa (25 ksi). These losses include those due to elastic shortening, shrinkage, creep, and relaxation, but exclude losses due to friction and anchorage slip. Branson and Kripanarayanan (1971) presented equations for predicting loss of prestress and camber in concrete members subject to either full or partial prestressing. Equations were given to account for the time-dependent effects of loss of prestress and the results were compared with experimental data. Simple empirical equations were provided by Meyers et al. (1972) for determining the long-term creep and shrinkage of concrete by comparison to experimental results. Prediction accuracy that previously required four months of testing could be achieved with only 28 days of creep and shrinkage data. Modifications of the lump sum method were subsequently included in the 1975 American Association of State Highway & Transportation Officials (AASHTO) Interim Specifications (AASHTO 1975). However, the treatment of losses as lumped sum quantities was recommended only for "standard" conditions. For members with unusual proportions, exceptionally long spans, or lightweight concrete, a separate estimate of the individual losses was recommended.

The Precast/Prestressed Concrete Institute (PCI) Committee on Prestress Losses (PCI 1975) issued in 1975 its "Recommendations for Estimating Prestress Losses." Both a general and a simplified method were presented for computing prestressing losses. In the general method, the total loss for post-tensioned construction was separated into one-time losses and time-dependent losses; the one-time losses included friction, anchorage, and elastic shortening, and the time-dependent losses were creep, shrinkage, and losses due to steel relaxation. Tadros et al. (1975) presented an analytical method to predict time-dependent prestressing losses, axial strain, and curvature at a section of a prestressed concrete beam or frame. The method covered non-composite pretensioned and post-tensioned structures. A step-by-step computer method was presented by Tadros et al. (1979) for predicting the stress distribution due to creep and shrinkage of concrete and relaxation of prestressing steel. Multipliers and design aids for predicting time-dependent deflections were presented by Tadros et al. (1985). The influence of creep and shrinkage of concrete, relaxation of prestressing steel, and the presence of nonprestressed steel on time-dependent deflection of prestressed concrete members were considered in the design aids. The PCI Handbook (PCI 2004) provides simple equations for estimating losses of prestress which would enable designers to estimate the various types of prestress loss rather than using a lump sum value. Although a number of methods are available for determining loss of prestress, these methods must be modified to be able to be used in post-tensioned concrete construction.

The state-of-the-art for spliced-girder bridges was reviewed by Abdel-Karim and Tadros (1993). A computer-based procedure for analysis of composite precast concrete girder bridges with cast-in-place topping was presented. The computer program evaluates stresses in concrete and steel at any cross-section in a statically indeterminate composite beam or plane frame, and gives the deflection at various stages of construction. Oh and Yang (2001) presented a method for improving long-term prediction of prestressing force changes in prestressed concrete structures. The method consisted of using short-term measurements in the field before opening the structure to traffic and then using the measurements to update predictions of prestress losses due to creep and shrinkage; the method was supported by statistical data. Camber and strains from 31 girders were recorded from time of prestressing force transfer to completion by Stallings

et al. (2003). An incremental time-step analysis was used to predict girder strains, camber, and prestressing losses up to the time of deck construction. The authors concluded that current analytical techniques are adequate, provided that the correct time-dependent material properties are appropriately integrated into the procedure. Wollmann et al. (2003) used the age-adjusted concrete modulus approach in the time-dependent analysis of spliced, precast concrete girder composite bridges. The approach allows designers to take advantage of higher concrete strength at time of post-tensioning and the resulting reduction in creep and shrinkage strains when determining prestressing losses for design.

A time-dependent loss method described in the AASHTO Load Resistance Factor Design (LRFD) Bridge Design Specifications (AASHTO 2004) is used in this paper to analyze the losses of a post-tensioned spliced girder at the anchorage zones and at midspan. The method is compared to measured losses through load cells at the anchorage zones and vibrating wire strain gauges at midspan. Predictions for the concrete modulus of elasticity, the ultimate creep coefficient, and ultimate shrinkage strain are compared to experiments carried out from the same concrete used to construct the post-tensioned spliced girder.

Actual tendon losses, which may be greater or smaller than the estimated losses, affect service load behavior such as deflection or camber, cracking load, and crack widths, as well as deformations during construction. Overestimation of losses, which may be seen to be on the conservative side, can actually be as detrimental as underestimation. Overestimation may lead the designer to specify too large of a prestressing force, which could result in excessive camber and shortening. It is thus necessary that the best possible estimate of losses be made.

Loss of prestressing force is considered using a time-dependent method based on the AASHTO LRFD Bridge Design Specifications (AASHTO 2004). The AASHTO total-loss method is not suitable for calculating losses in the present case, since it does not take into account the concrete age at the time of post-tensioning and the presence of a precompressed deck supported on shored, post-tensioned spliced girders. The effect of light pretensioning of the girder segments was ignored in the calculation of losses. The pretensioning was carried out mainly for erection purposes and was limited to individual girder segments; as such, the contribution from the pretensioning strands to losses is small compared to the losses from post-tensioning of the spliced girder. The precast concrete deck sections measured 2.438 m (8 ft) square and were 90 mm (3.5 in.) thick, with a design compressive strength equal to 35 MPa (5 ksi). The thickness of the cast-in place concrete deck was 125 mm (4–5/16 in.) with concrete of a design compressive strength equal to 35 MPa (5 ksi); thus, the overall thickness of the deck was 215 mm (8-7/16 in.). In addition, the girder spacing was 3.337 m (10 ft 11-3/8 in.).

Time-dependent losses were calculated for a period of three years and eight months, corresponding to the monitoring period of the instrumented girder. Time increments were initial losses, every week for a period of three months after post-tensioning, and every month for the remaining period until December 31, 2003 (3 years and eight months or 3.7 years). Losses considered were elastic shortening, creep, shrinkage, tendon relaxation, anchorage seating, and friction loss, which were added to give the total loss.

8. AASHTO LRFD TIME-DEPENDENT LOSS METHOD

Elastic Shortening Loss

The elastic shortening of concrete loss for post-tensioned girders depends on the sequence of jacking. In the present case, Tendon #1 at the top was stressed first, followed by Tendons #2, #3, and #4. In general, if N is the number of tendons that are sequentially tensioned, the elastic shortening loss is given as (Nawy 2003):

$$\Delta f_{ES} = \left(\frac{1}{N}\right) \sum_{j=1}^{N} \left(\frac{E_{ps}}{E_{ci}}\right) f_{cs} \tag{5}$$

where j = number of jacking operations, which in this case is equal to four; E_{ci} = modulus of elasticity of concrete at transfer, calculated using Eq. (2) with $f_c^{'}$ = 82 MPa (11.9 ksi); E_{ps} = modulus of elasticity of prestressing steel (193 GPa or 28x10^6 psi); and f_{cs} = stress in the concrete at the tendon centroid. Total losses due to elastic shortening were: Tendon #1 = 100.3 MPa (14.5 ksi), Tendon #2 = 66.9 MPa (9.7 ksi), Tendon #3 = 33.4 MPa (4.8 ksi), and Tendon #4 = 0.0 MPa (0.0 ksi). Tendon #4 (bottom) was tensioned last and did not suffer any losses due to elastic shortening; Tendon #1, which was tensioned first, suffered the maximum amount of loss.

Time-dependent Creep Loss

In establishing creep loss, the time-dependent properties of concrete were not considered, because when the girder was post-tensioned, the concrete was 134 days old with a measured compressive strength of 82 MPa (11.9 ksi) at 90 days. Creep loss occurred in the girder after post-tensioning, which was performed after the deck was cast. The effective area of concrete was included in the calculation of the creep coefficient; the volume-to-surface (V/S) ratio used was based on an average value of the girder section and the girder plus deck combined section.

The time-dependent creep coefficient according to the AASHTO LRFD Specifications (AASHTO 2004) is defined as:

$$\psi(t,t_i) = 3.5 k_c k_f \left(1.58 - \frac{H}{120}\right) t_i^{-0.118} \frac{(t-t_i)^{0.6}}{10.0 + (t-t_i)^{0.6}} \tag{6}$$

where t = maturity of concrete (day), t_i = age of concrete when load is initially applied (day), H = relative humidity (%) taken as 50%, and k_f = factor for the effect of concrete strength given as:

$$k_f = \frac{62}{42 + f_c^{'}} \text{ (MPa)}; \quad k_f = \frac{9}{6 + f_c^{'}} \text{ (ksi)} \tag{7}$$

where $f_c^{'}$ = specified concrete strength at 28 days measured as 75.8 MPa (11.0 ksi), and k_c = time-dependent factor for the effect of volume-to-surface ratio, given as:

$$k_c = \left[\frac{t}{\dfrac{26e^{0.0142(V/S)}+t}{\dfrac{t}{45+t}}}\right]\left[\frac{1.80+1.77e^{-0.0213(V/S)}}{2.587}\right] \text{ (mm);}$$

$$k_c = \left[\frac{t}{\dfrac{26e^{0.36(V/S)}+t}{\dfrac{t}{45+t}}}\right]\left[\frac{1.80+1.77e^{-0.54(V/S)}}{2.587}\right] \text{ (in.)} \quad (8)$$

An average value of V/S = 100 mm (4 in.) was used, as described earlier. The loss due to creep can be found from the expression (Nawy 2003):

$$\Delta f_{CR}(t) = \psi(t,t_i)\frac{E_{ps}}{E_c} f_{cs} \quad (9)$$

where f_{cs} is the stress in the concrete at the level of the centroid of the tendon, given as (Nawy 2003):

$$f_{cs} = -\frac{P_i}{A_c}\left(1+\frac{e^2}{r^2}\right)+\frac{M_D e}{I_c} \quad (10)$$

where A_c, I_c and r are the area, moment of inertia and radius of gyration of the girder section, e is the tendon eccentricity, and M_D *is* the bending moment due to total superimposed load. Creep recovery due to loss of prestress was accounted for in the calculation of creep loss in the stress at the center of gravity of the strands; in calculating f_{cs}, the axial load P_i was reduced as the prestress loss was reduced, thus adjusting the creep loss as other losses (and prior creep losses) accumulated.

Time-dependent Shrinkage Loss

According to the AASHTO LRFD Specifications (AASHTO 2004), for steam-cured concrete the strain due to shrinkage at time t is given as:

$$(\varepsilon_{sh})_t = -k_s k_h\left(\frac{t}{55.0+t}\right)0.56x10^{-3} \quad (11)$$

where, t = drying time (day), k_s = size factor, the value of which depends on the volume-to-surface ratio as:

$$k_s = \left[\frac{t}{\dfrac{26e^{0.0142(V/S)} + t}{\dfrac{t}{45+t}}} \right] \left[\frac{1064 - 3.70(V/S)}{923} \right] \text{ (mm);}$$

$$k_s = \left[\frac{t}{\dfrac{26e^{0.36(V/S)} + t}{\dfrac{t}{45+t}}} \right] \left[\frac{1064 - 94(V/S)}{923} \right] \text{ (in.)} \qquad (12)$$

A value of V/S = 100 mm (4 in.) was used as described in the section on creep loss; k_h = humidity factor based on the annual ambient relative humidity; here a value of 50 % relative humidity was used, which resulted in a value of k_h = 1.29. The loss due to shrinkage can be found from the expression (Nawy 2003):

$$\Delta f_{SH}(t) = (\varepsilon_{sh})_t E_{ps} \qquad (13)$$

Time-dependent Steel Stress Relaxation Loss

Relaxation losses of prestressing tendons after transfer may be defined according to the following expression from the PCI *Committee on Prestress Losses General Method* (PCI 2004):

$$\Delta f_R(t) = f'_{pi} \left(\frac{\log t'}{45} \right) \left(\frac{f'_{pi}}{f_{py}} - 0.55 \right) \qquad (14)$$

where f'_{pi} = initial stress in the tendon at the end of stressing taken as $0.70f_{pu}$; f_{pu} = specified tensile strength of prestressing steel taken as 1860 MPa (270 ksi); f_{py} = yield strength of prestressing steel taken as $0.9f_{pu}$; and t' = time, in hours, over which relaxation is considered. It should be noted that the removal of the erection (shoring) towers affected the strain in the girders, but it had no effect on the losses, since the post-tensioning lifted the girders off the towers, thereby not causing any stresses.

Anchorage-seating Loss

Losses due to anchorage-seating are calculated based on an estimated slip of 10 mm. The assumption of a slip Δ_A = 10 mm, also referenced in AASHTO (2004), resulted in an anchorage loss given as:

$$\Delta f_{PA} = \frac{\Delta_A}{L} E_{ps} \qquad (15)$$

where L = tendon length, and E_{ps} = modulus of elasticity of prestressing reinforcement. The length of tendon affected by anchorage set was considerably less than half the girder span and thus this loss did not affect the calculation of losses at midspan.

Friction Losses

Losses due to friction between the internal tendon and the duct wall were calculated according to the expression (Collins and Mitchell 2003):

$$\Delta f_{pF} = f_{pj}\left(1 - e^{-(Kx+\mu\alpha)}\right) \tag{16}$$

where f_{pj} = stress in the prestressing steel at jacking; x = length of a prestressing tendon from the jacking end to any point under consideration; K = wobble friction coefficient per unit length of tendon; μ = coefficient of friction; α = sum of the absolute values of angular change of prestressing steel path from jacking end to the point under investigation; for example from the jacking end to midspan, $\alpha = 4y' / L_g$, where y' = total vertical change of tendon path, i.e. height of tendon at girder end minus height of tendon at girder midspan, and L_g = girder span.

The measurements taken were not sequenced correctly so that the coefficient of friction (μ) and the wobble friction coefficient (K) could not be found for evaluating friction losses. However, Wollmann, et al. (2003) have recently provided site specific data for μ and K for a similar girder located at the 7200 South I-15 overpass in Salt Lake City which is near the location of the bridge used in the present study. The 7200 South bridge was constructed using the same girder cross-section and with the same post-tensioning method. The testing reported by Wollmann, et al. (2003) recommended a friction coefficient of 0.25 and a wobble coefficient of 7×10^{-7}/mm (1.778×10^{-5} /in.) which were used in the calculations.

9. COMPARISON OF AASHTO LRFD TIME-DEPENDENT LOSS METHOD TO EXPERIMENTAL MEASUREMENTS

The total losses using the time-dependent method are shown in Tables 7-9 for the four tendons at seating, after ½ year, 1 year, 2 years, and 3.7 years. Table 7 compares the time-dependent losses to the measured losses from load cells at the jacking end; Table 8 compares the time-dependent losses to the measured losses from load cells at the anchored end; and Table 9 compares the time-dependent losses to the measured losses from vibrating wire strain gauges at midspan. The 3.7 years benchmark corresponds to the last day of experimental load cell measurements of December 31, 2003.

Table 7 shows that Tendon T4 (bottom) has the smallest losses from the measurements at the jacking end (LC-4) confirming the time-dependent method prediction. The time-dependent method overestimates the losses obtained from the load cells (except load cell 4 which shows erratic readings); at 3.7 years, this overestimation ranges between 2.4% and 6.1% of the total losses. Table 1.8 shows too that Tendon T4 (bottom) has the smallest losses from the measurements at the jacking end (LC-8) confirming the time-dependent method prediction; as

Table 7. Time-dependent losses compared to measured losses from load cells at jacking end.

Time (yrs)	T1-C (%)	T2-C (%)	T3-C (%)	T4-C (%)	LC-1 (%)	LC-2 (%)	LC-3 (%)	LC-4 (%)
½	18.5	15.3	12.8	10.0	10.5	9.8	8.0	6.5
1	20.2	17.0	14.5	11.6	12.0	10.8	9.0	7.2
2	21.7	18.4	15.9	12.9	14.2	12.4	10.6	-
3.7	22.6	19.3	16.8	13.8	16.5	13.8	14.4	-

Ti-C = Calculated Prestressing Force in Load Cell 'i'
LC-i = Measured Prestressing Force from Load Cell 'i'

Table 8. Time-dependent losses compared to measured losses from load cells at anchored end.

Time (yrs)	T5-C (%)	T6-C (%)	T7-C (%)	T8-C (%)	LC-5 (%)	LC-6 (%)	LC-7 (%)	LC-8 (%)
½	20.5	16.8	14.0	10.8	9.9	7.9	8.0	6.7
1	22.5	18.7	15.8	12.5	11.3	9.2	9.2	-
2	24.1	20.2	17.3	13.9	13.0	10.8	11.2	-
3.7	25.2	21.3	18.3	14.9	14.8	12.9	12.6	-

Ti-C = Calculated Prestressing Force in Load Cell 'i'
LC-i = Measured Prestressing Force from Load Cell 'i'

Table 9. Time-dependent losses compared to measured losses from vibrating wire strain gauges at midspan.

Time (yrs)	TC-1 (%)	TC-2 (%)	TC-3 (%)	TC-4 (%)	VW-1 (%)	VW-2 (%)	VW-3 (%)	VW-4 (%)
½	17.9	14.6	11.9	11.4	12.3	12.0	12.1	11.4
1	19.8	16.4	13.7	13.0	13.2	12.8	12.9	12.7
2	21.3	17.8	15.1	14.4	13.9	13.6	13.7	13.5
3.7	22.3	18.8	16.1	15.2	14.8	14.4	14.5	14.3

TC-x = Calculated Prestressing Force in Tendon 'x'

LC-x = Measured Prestressing Force from Vibrating Wire Strain Gauge 'x'
for the jacking end, the time-dependent method overestimates the losses obtained from the load cells (except load cell 8 which shows erratic readings); at 3.7 years, this overestimation ranges between 5.7% and 10.4% of the total losses. Table 9 shows that Tendon T4 (bottom) has the smallest losses from the measurements at midspan (VW-4) confirming the time-dependent method prediction; at 3.7 years, the time-dependent method overestimates the losses obtained from the vibrating wire strain gauges by 0.9% to 7.5% of the total losses.

Figure 19 shows the tendon forces remaining after losses at the jacking end using the time-dependent method; Figure 19 also shows the actual measured tendon forces from load cell readings at the jacking end (north abutment anchorage zone); the time-dependent method predicts the prestressing forces in a satisfactory manner, except for load cell 4 which shows erratic readings after 1.5 years. Figure 20 shows the tendon forces remaining after losses at the anchored end using the time-dependent method; Figure 20 also shows the actual measured tendon forces from load cell readings at the anchored end (south abutment anchorage zone); the prediction from the time-dependent method is less satisfactory than the jacking end but it is still conservative, except for load cell 8 which shows erratic readings. The tendon forces remaining after losses at midspan using the time-dependent method are shown in Figure 21; these are compared to the tendon forces obtained from actual vibrating wire strain gauge readings at midspan. From Figure 21, it can be seen that the time-dependent method predicts the prestressing forces conservatively for all four tendons.

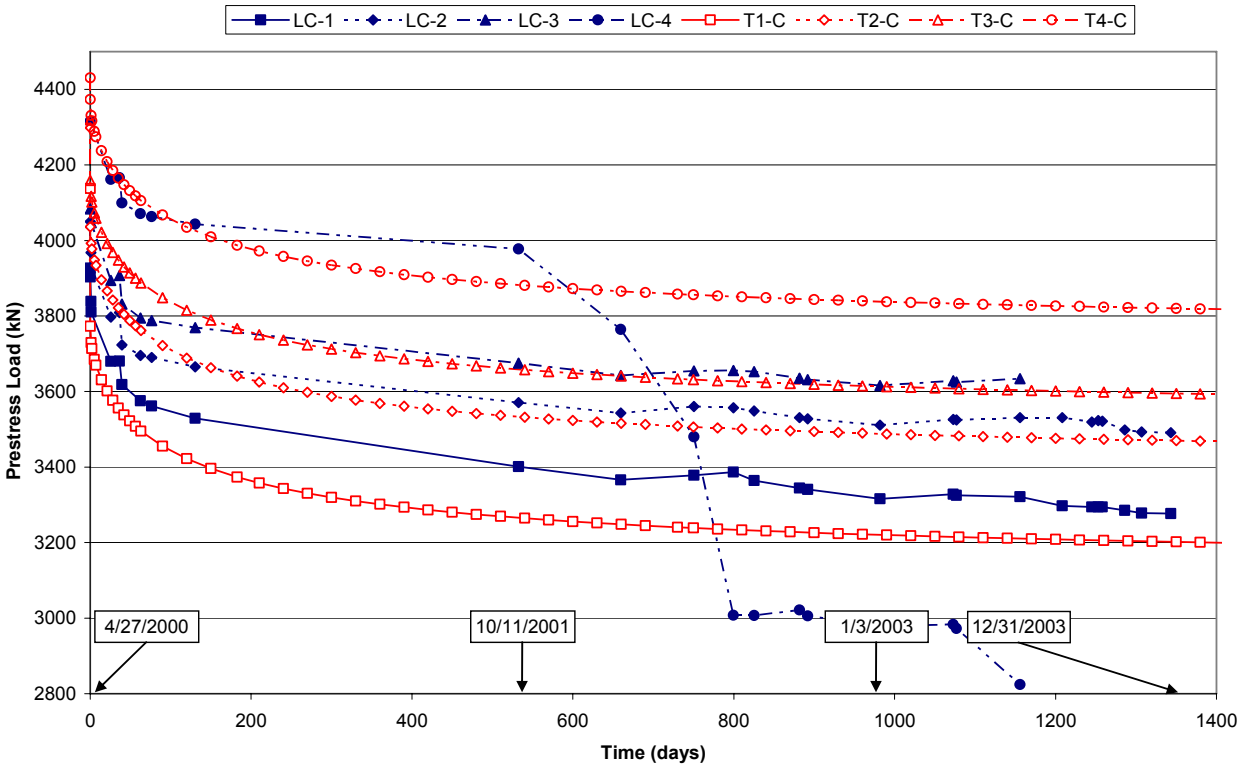

Figure 19. Effective prestressing force at jacking end: time-dependent method (T1-C, T2-C, T3-C, T4-C) vs. measurements from load cells (LC-1, LC-2, LC-3, LC-4).

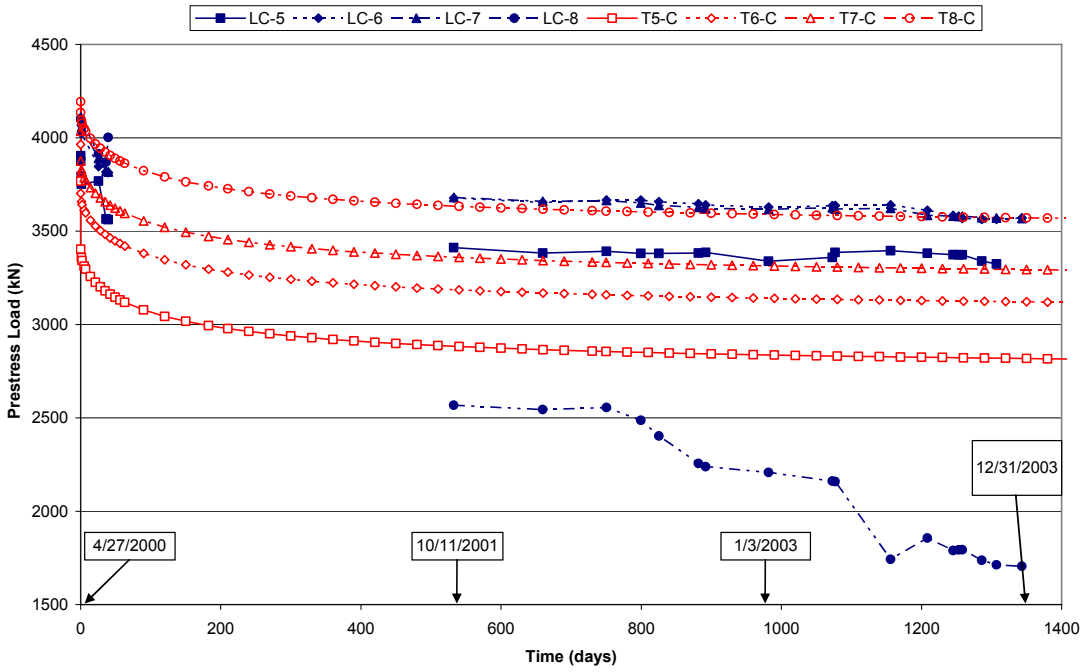

Figure 20. Effective prestressing force at anchored end: time-dependent method (T5-C, T6-C, T7-C, T8-C) vs. measurements from load cells (LC-5, LC-6, LC-7, LC-8).

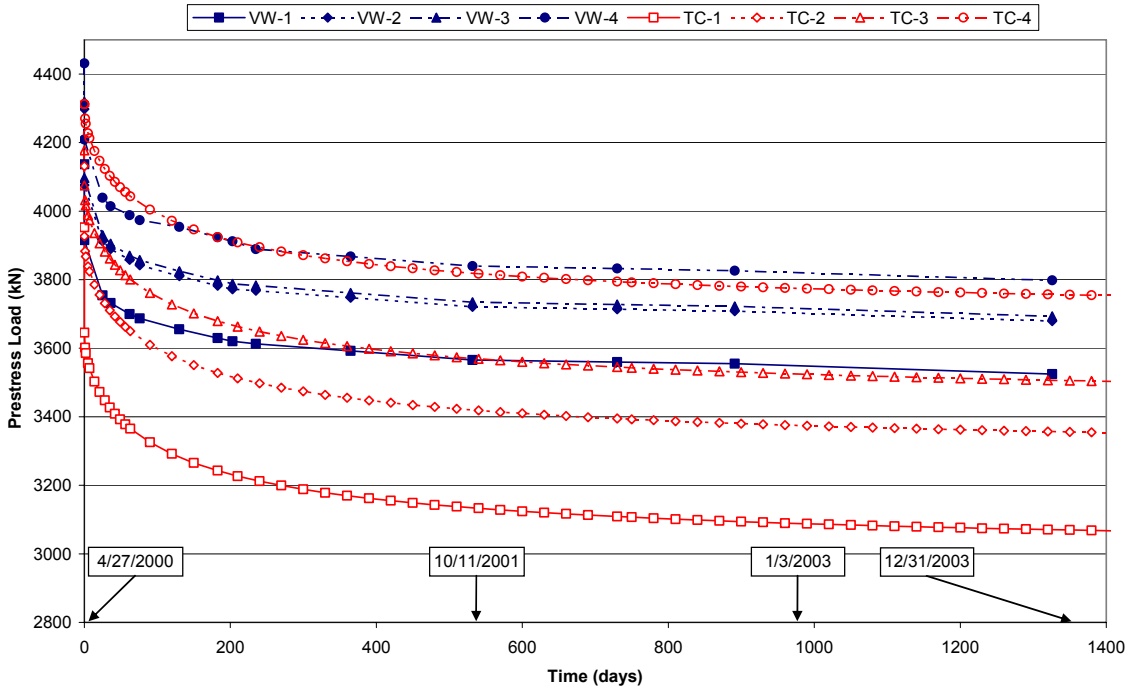

Figure 21. Effective prestressing force at midspan: time-dependent method (TC-1, TC-2,

TC-3, TC-4) vs. measurements from vibrating wire strain gauges (VW-1, VW-2, VW-3, VW-4).

10. COLD JOINTS BETWEEN PRECAST CONCRETE PANELS FOR CONSTRUCTION OF THE DECK

To measure possible cracks at the cold joints of the precast concrete deck panels, special instrumentation was installed. The precast panels of the deck were instrumented with Linear Variable Differential Transducers (LVDTs) across certain joints. These LVDTs measure deflection between adjacent panels. Two vertical LVDTs and one horizontal LVDT were installed on the bridge. Vertical LVDTs measure differential deflection in the vertical plane parallel to the panel joint, while the horizontal LVDT measures the effects of the panels moving into or moving away from one another. These instruments are mounted securely to one side of a precast panel joint such that the spring loaded actuator extends across the joint enabling relative displacements to be measured. The method of mounting the vertical and horizontal gauges is shown in Figures 22 and 23.

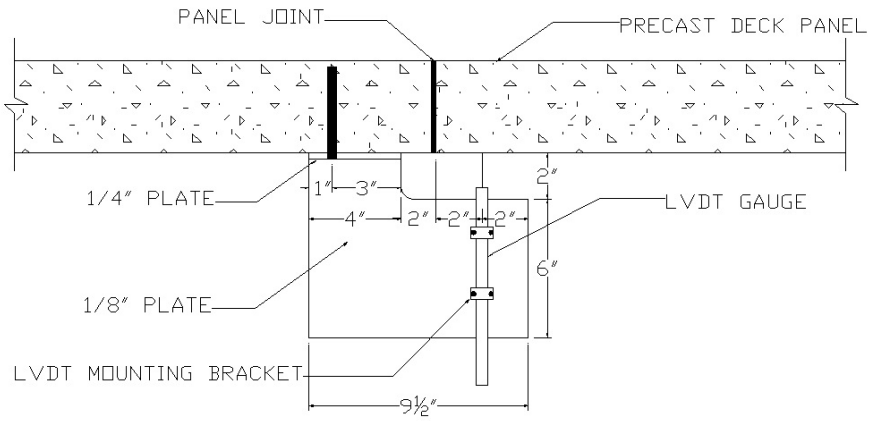

Figure 22. Schematic of Vertical LVDT Mounting (1in. = 25.4 mm).

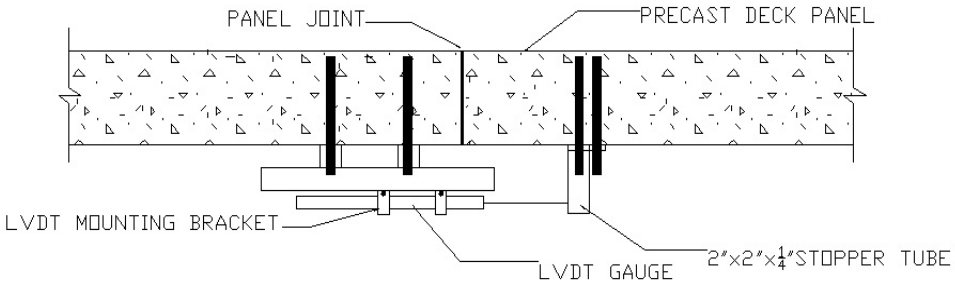

Figure 23. Schematic of Horizontal LVDT Mounting.

The LVDT instruments used in this research are capable of measuring displacements at a rate of 10,000 scans per second; scan rates of 100 or 1,000 scans per second were used to enable longer scan intervals. The instruments were installed near the north abutment at the midspan of the panels (i.e. midway between two adjacent girders). A cross section of the bridge showing the location of LVDTs relative to the lanes of traffic above is shown in Figure 24.

The placement of LVDTs shown in Figure 24 was determined by three factors: First, the lanes above should be as closely centered over the supporting girders as possible. Second, the LVDTs should be placed such as to be subjected to the most ideal combination of frequency and load of traffic. Thus, LVDTs #2 and #3 were placed under the third lane from the left where the most desirable combination of automobiles and trucks was observed. Finally, it was desirable to instrument a cold joint that appeared to have an indication of penetration of water. The cold joint under the fourth lane from the left appeared to be the most questionable and LVDT 1 was placed at this point; LVDT #2 (vertical) and #3 (horizontal) are shown in Figure 25.

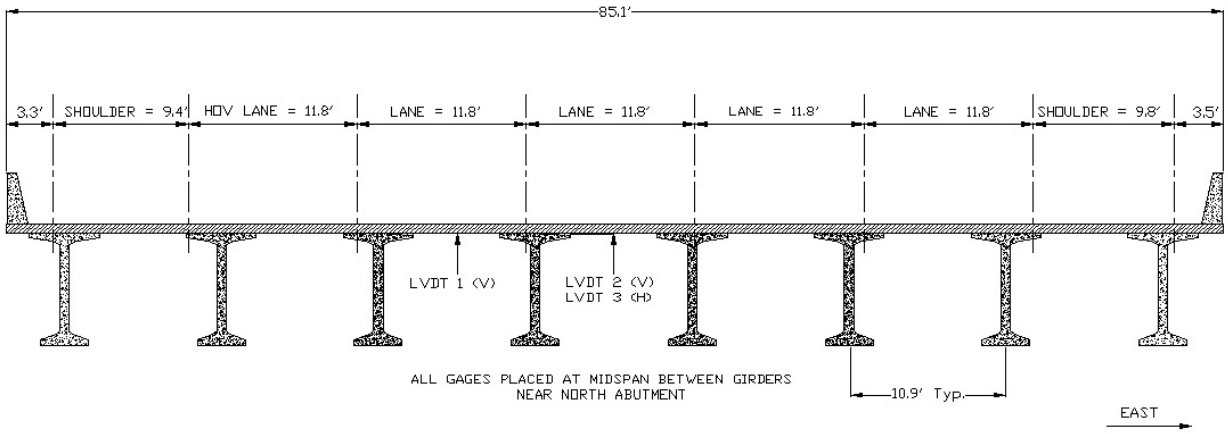

Figure 24. Locations and Orientations of LVDT Gauges (North into Page) (1 ft = 205 mm).

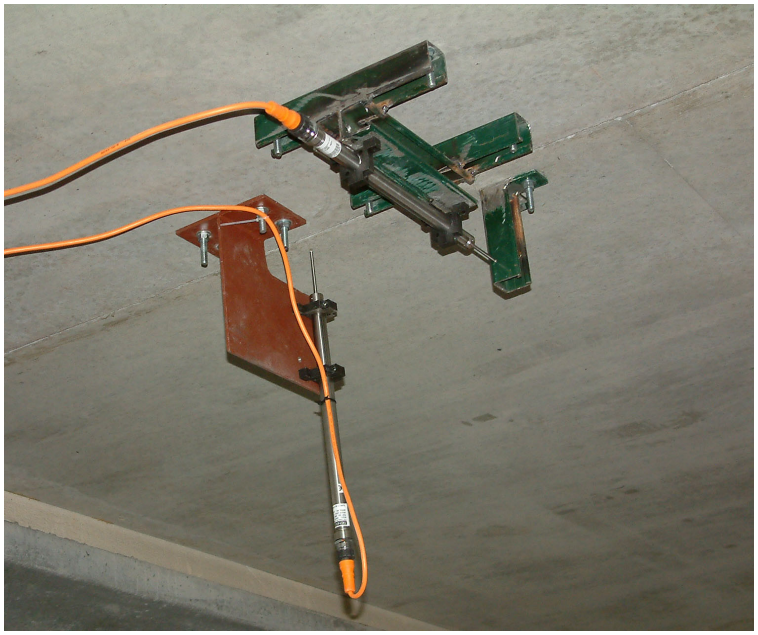

Figure 25. LVDTs #2 and #3.

Truck Load Test

On August 19, 2003 a truck load test was preformed on the northbound bridge of the I-15 4500 South overpass. The test began at 11:30 pm and continued for approximately 1.5 hours. The test included both a static test, where two loaded trucks were stationary at a point for a given time, and two high speed passes over the bridge at 25 and 40 miles per hour. To test the performance of the precast deck panel joints, two high speed passes were made over the section of the bridge that is measured by the LVDT gauges shown in Figure 24. The LVDT gauge measurements were read at an interval of 10,000 readings per second. The gauges are mounted to the underside of the deck, directly to the precast panel. The orientations of these gauges are shown in Figures 22, 23, and 25. High speed passes were made over this section of deck at 25 miles per hour (MPH) and 40 MPH.

LVDT readings for the high speed passes are shown in Figures 26-28 for the 25 MPH test and in Figures 29-31 for the 40 MPH test. The exact time when the trucks passed over the actual joint measured by the LVDTs is not known, although the 50 second time range of the test is clearly enough time for the trucks to travel across the bridge at 40 or 25 miles per hour. A vehicle traveling at 40 miles per hour would take approximately 3.4 seconds to travel across the 200 feet of the bridge span. At 25 miles per hour, the travel time would be approximately 5.5 seconds. Thus the figures may be examined for "spikes" or other abnormalities which would indicate the presence of the truck-loading acting on the joint being measured. In addition, if there are noticeable spikes, they should be evident in some form in the other figures of the same test (25 MPH or 40 MPH) at the same time since all three LVDTs started recording data at precisely the same time.

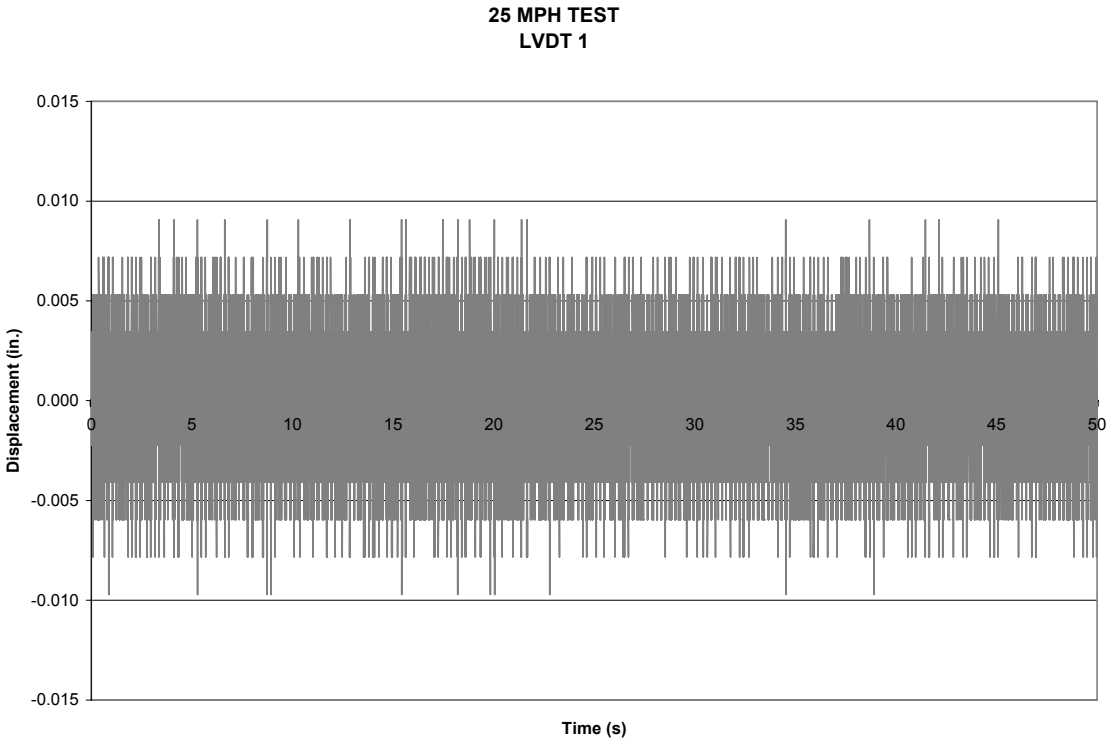

Figure 26. Joint Displacement Measurements from LVDT 1 During 25 MPH Test.

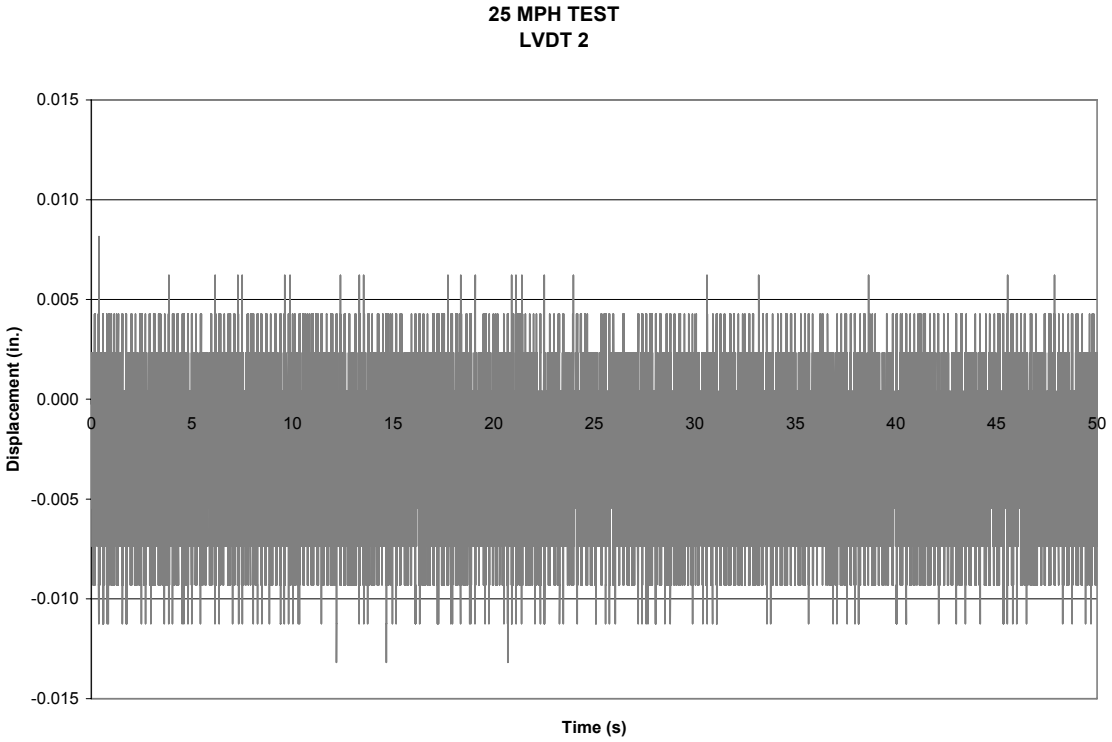

Figure 27. Joint Displacement Measurements from LVDT 2 During 25 MPH Test.

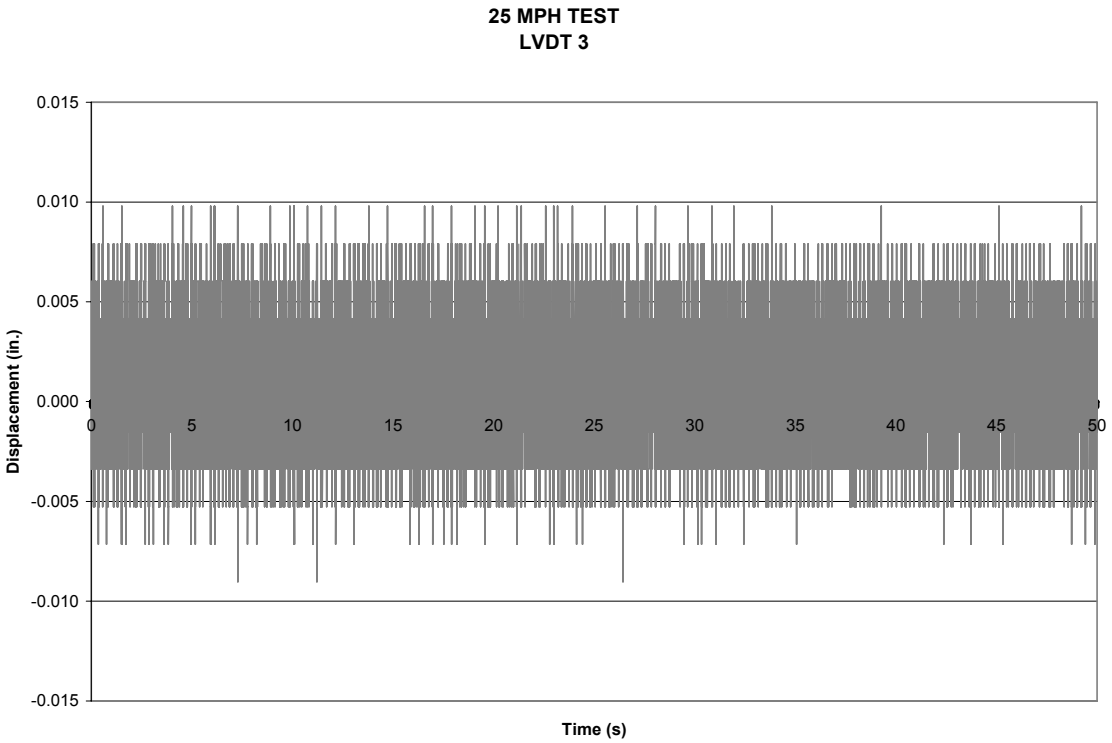

Figure 28. Joint Displacement Measurements from LVDT 3 During 25 MPH Test.

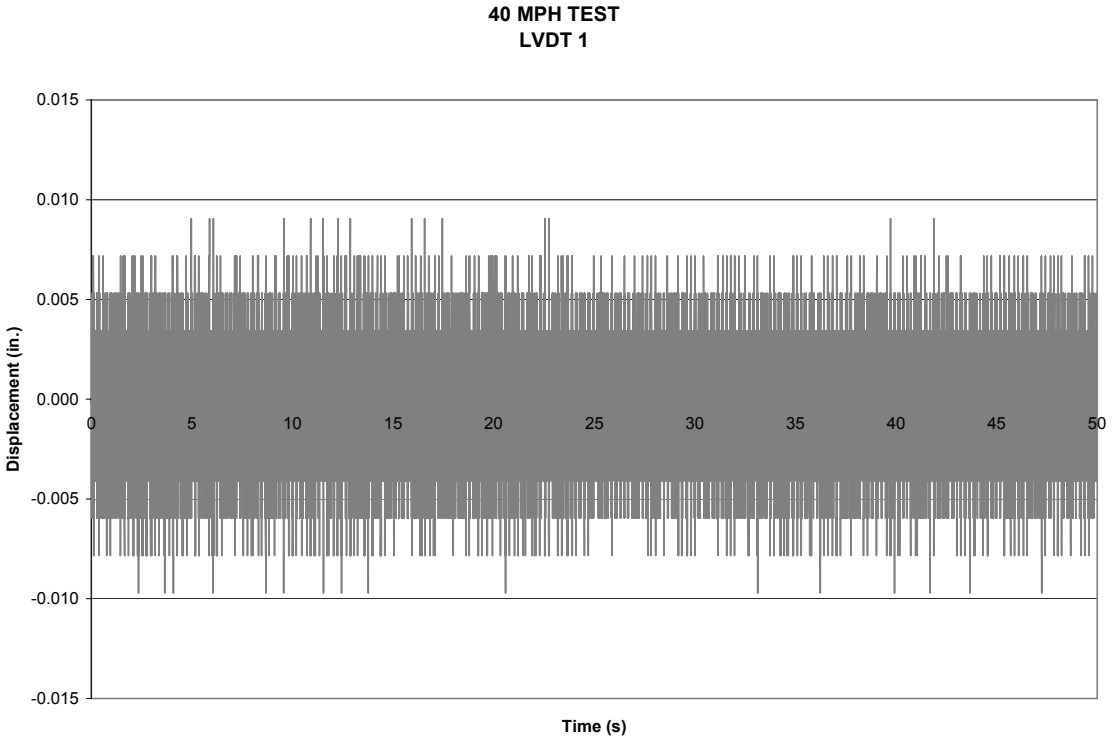

Figure 29. Joint Displacement Measurements from LVDT 1 During 40 MPH Test.

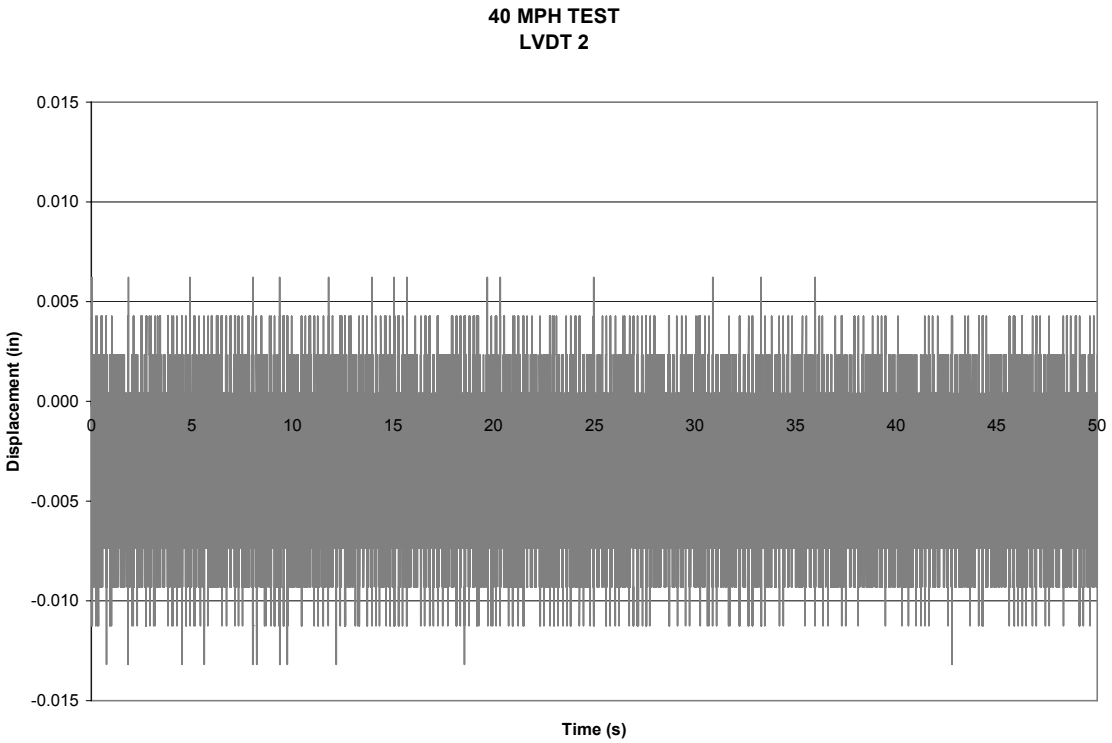

Figure 30. Joint Displacement Measurements from LVDT 2 During 40 MPH Test.

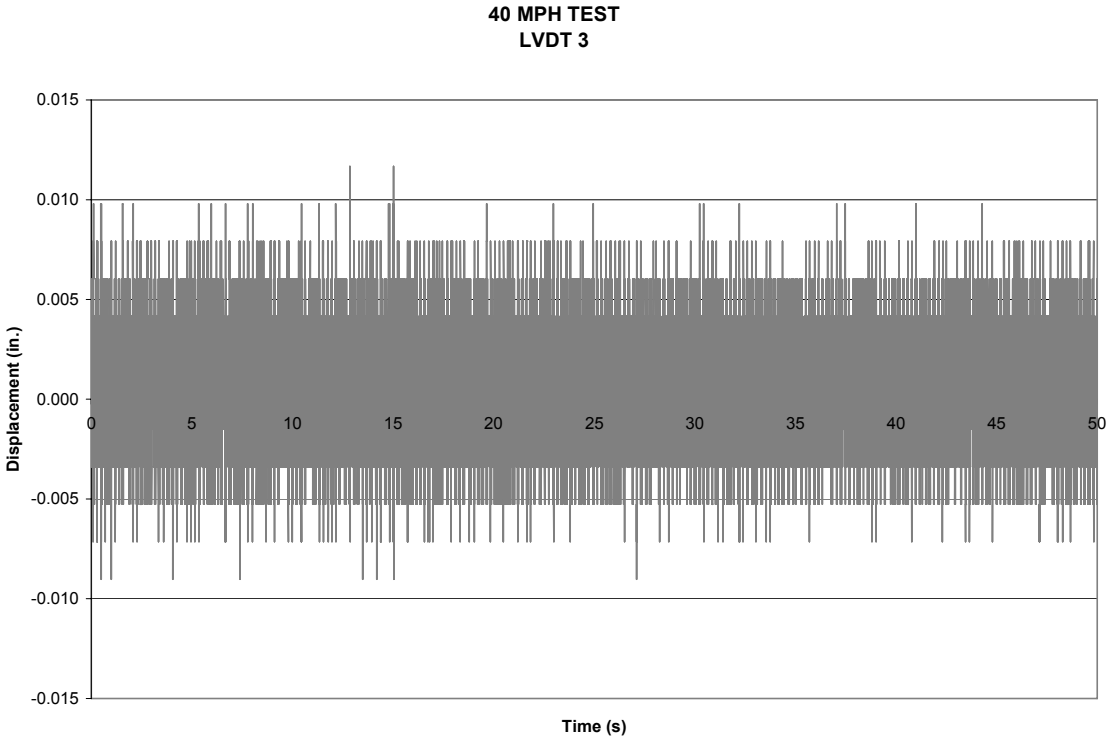

Figure 31. Joint Displacement Measurements from LVDT 3 During 40 MPH Test.

Examination of Figures 26-28 during the 25 MPH test and Figures 29-31 during the 40 MPH test clearly shows that there is little evidence of any displacement above the "noise" level of the instruments. In neither set of figures can a 3.4 or 5.5 second period be seen that is significantly different than the rest of the figure. Additionally, there is no instance of a "spike" in displacement which shows up as a "spike" at the same time instance on another figure from the same test. These facts would indicate that the precast panels are performing adequately and are not cracking at the cold joints; this is due to the large prestressing force, and the diaphragm action of the deck and intermediate splice diaphragms.

Long Term Ambient Measurements

On January 22, 2004, at 2:00 pm another set of measurements was taken from LVDTs 1-3 under ambient loads from traffic. It is clear that the range of the displacement from these readings is within the same magnitude as the readings obtained from the truck load test. The range of displacements is between 15-21 thousands of an inch (0.38 mm – 0.53 mm). The cold joints are behaving as they did during the truck load tests and are believed to be in good health. Moreover, the lack of deck cracking in this bridge as compared to the decks of steel girder bridges makes this a successful system. During observations under rainy conditions, no water was observed below the deck.

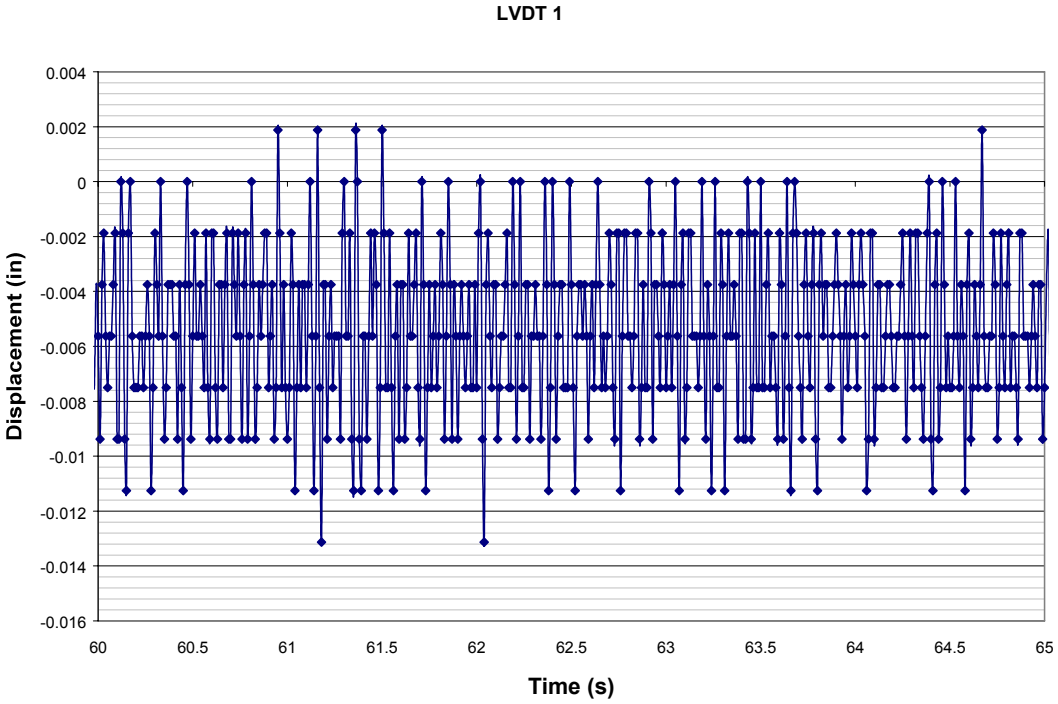

Figure 32. Joint Displacement Measurements by LVDT 1 from traffic.

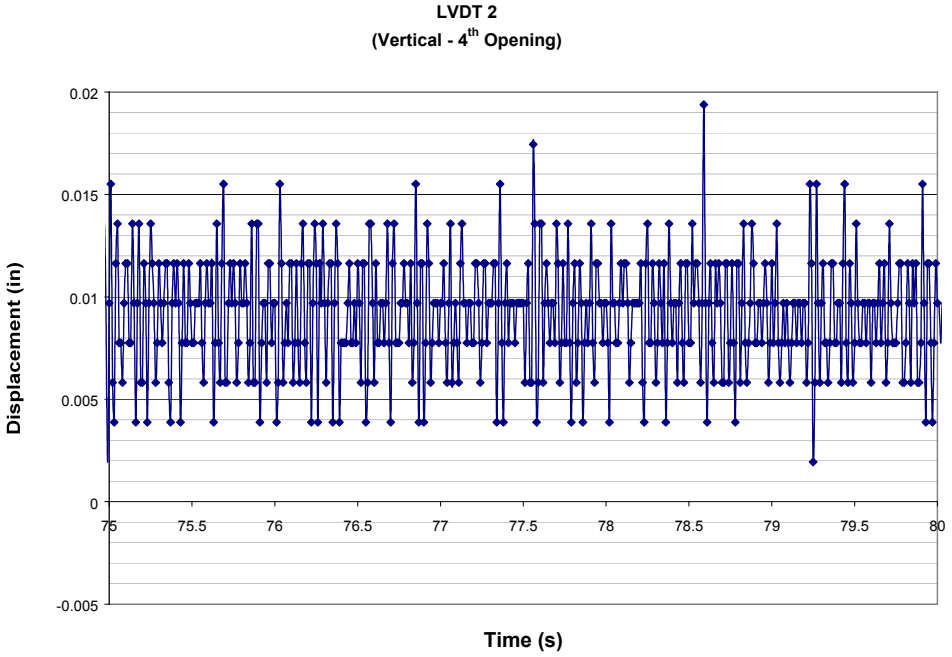

Figure 33. Joint Displacement Measurements by LVDT 2 from traffic.

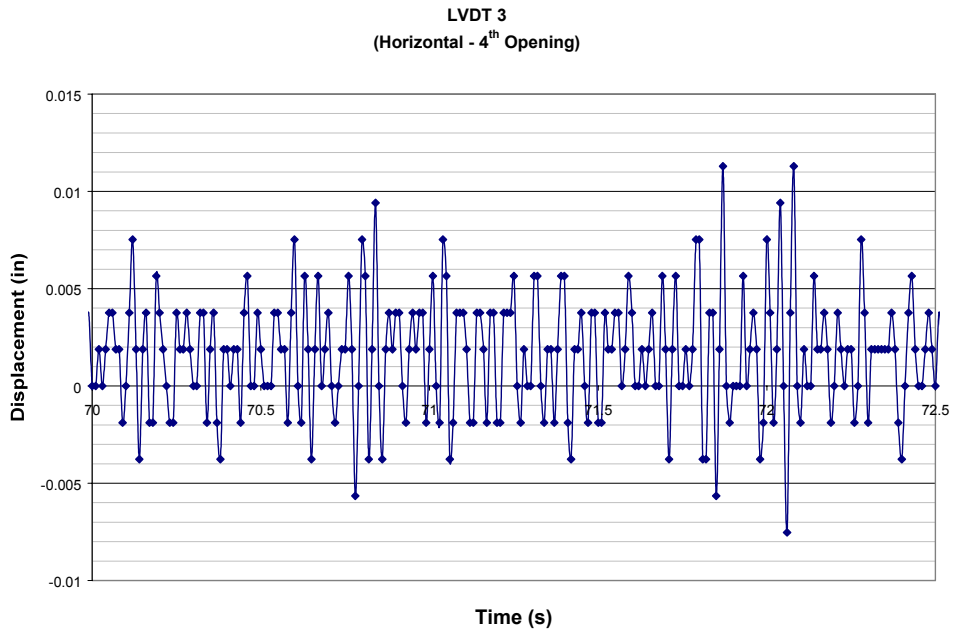

Figure 34. Joint Displacement Measurements by LVDT 3 from traffic.

11. DEFLECTIONS OF POST-TENSIONED SPLICED GIRDER "A" FROM SURVEY MEASUREMENTS

Survey measurements have been taken of the deflected shape of Girder A and of the north and south end-abutments. Beginning in April 2000, survey measurements of the bridge were made at various intervals. Measurements were made at multiple times during the same day to account for temperature differences. Initially, measurements were made many times a month; during the final 14 months of this study, survey measurements were made every two months. Each time measurements were made during this 14 month period, a morning, noon, and afternoon reading was taken. Seven survey points were originally placed on the parapet above Girder A beginning at the north end abutment; two survey points are located above the north and south end abutments, with one survey point at midspan. Two survey points are located at the center of the north and south end segments, and two survey points are located at the north and south splices.

Figure 35 shows the increase of upward deflections in the early days following post tensioning of Girder A. On May 2, 2000, after tensioning of the eight spliced girders of the Northbound Bridge was completed, the upward deflection of Girder A at midspan was 53 mm (2 in.); at the time the south end-abutment was placed, on May 23 2000, this deflection was 53 mm (2 in.), and at the time the north end-abutment was placed on June 3, 2000, this deflection was 56 mm (2 in.). It should be noted that the abutments are semi-integral and that they are supported on 406 mm (16 in.) concrete-filled steel pile pipes. Figure 35 shows that the north end-abutment near the end of the monitoring period, on December 8, 2003 had experienced 23 mm (0.9 in.) of settlement while the south end-abutment had settled 30 mm (1.2 in.). The settlement is coming from the clay layers that underlie this site and are found beneath the stratum of the piling. A 25 mm (1 in.) settlement of a pile-supported bridge is typical for this area; as a reference, the adjacent embankment was designed to settle about 75 mm (3 in.) in 10 years.

The maximum upward deflection recorded at midspan was 67 mm (2.6 in.) on June 3, 2003, which corresponds to an absolute deflection in the span of 91 mm (3.6 in.), or a ratio of (clear span)/679; at this time the north and south end-abutments had settlements of 23 mm (0.9 in.) and 25 mm (1 in.), respectively.

The deflected profile of the spliced girder is approximately parabolic, as shown in Figure 36; while the deflection has varied with time and temperature, it has stabilized after 3 years and 8 months**.** Figures 35 and 36 confirm that the deflection of the two splice points is practically the same. The elevations of the north and south splice survey points have not varied by more than 4 mm (0.2 in.) from each other and on average the points have varied by only 1 mm (0.04 in.). The midspan point (Pt 4) has typically followed the deflection of the splice points, as expected; the difference between midspan and either splice diaphragm deflection was in the range of 10 to 17 mm (0.4 to 0.7 in.). The average difference between the midspan and splice deflections was 16 mm (0.6 in.). The midspan upward deflection has been in the range of 8% to 43% higher than the splice points, with the average upward deflection being 25% higher than that of the splice points.

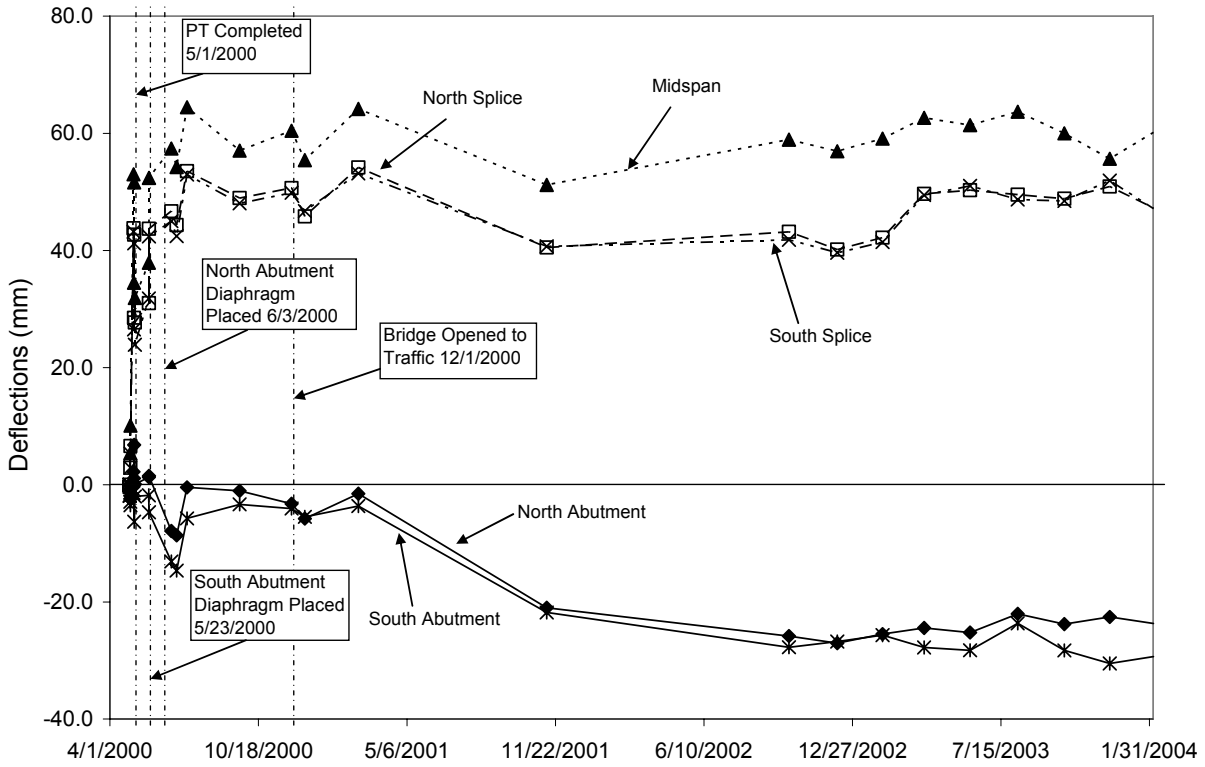

Figure 35. Girder A deflections versus time (1 in. = 25.4 mm)

Figures 35 and 36 indicate that the midspan deflection began stabilizing after December 2002, showing that variation in deflection is associated primarily with creep effects. The end abutments have experienced an average of 27 mm (1.1 in.) of settlement during the 44 month study period. Even though the south-end abutment has experienced a 35% larger settlement than the north–end abutment, the two splices have experienced practically identical deflections. The coincidence of the deflection of the two splice points in a single clear span of 61.443 m (201 ft-7 in.) indicates excellent girder/splice performance. This was also verified by the tiltmeters which showed no differential rotation occurring at the splice in the plane of the girder.

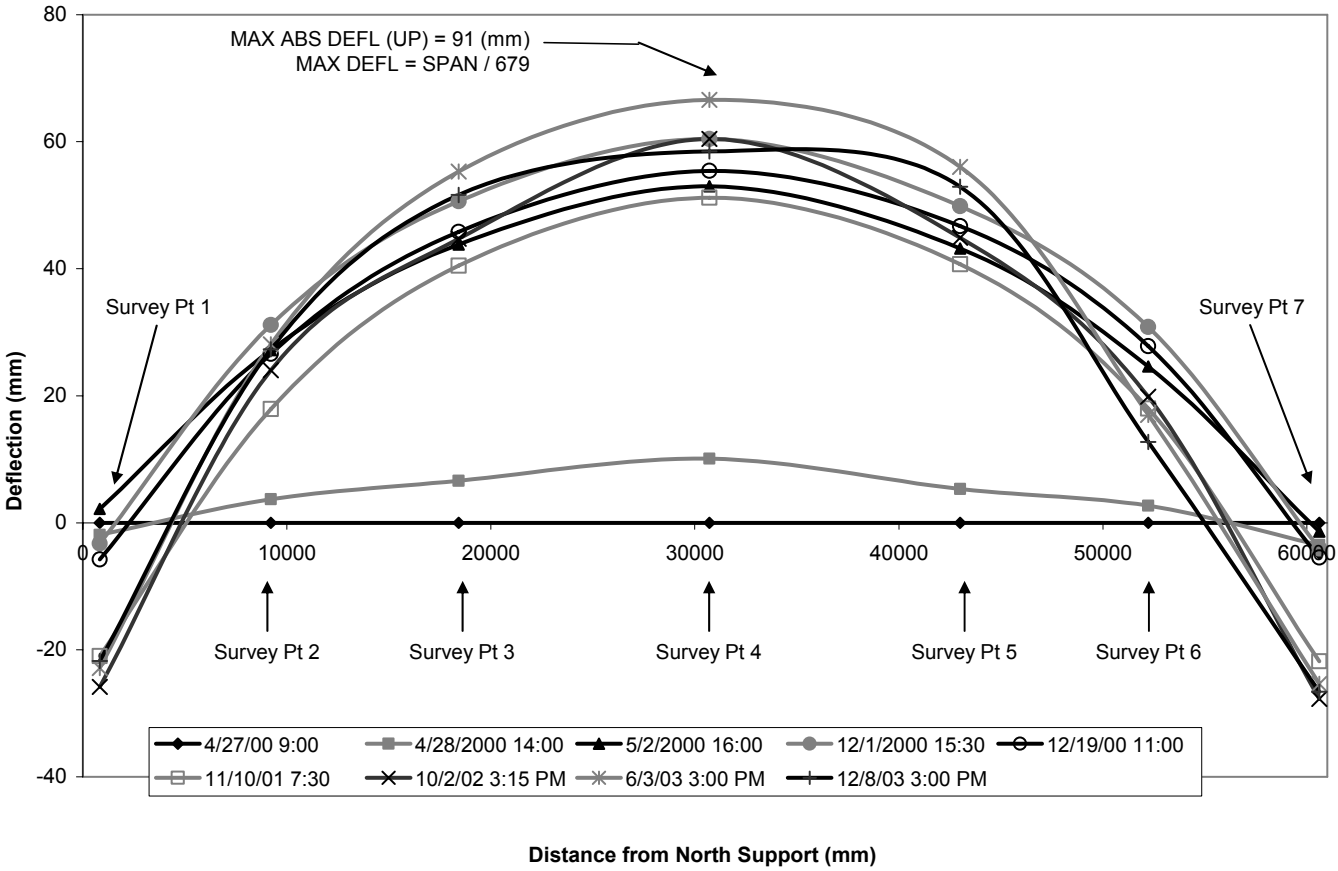

Figure 36. Profile of Girder A deflections at various times (1 in. = 25.4 mm)

12. DEFLECTIONS OF POST-TENSIONED SPLICED GIRDER "A" DUE TO TEMPERATURE VARIATIONS AND COMPARISON TO AASHTO PREDICTIONS

The AASHTO LRFD Bridge Design Specifications (AASHTO 2004) Section 3.12.3 explains how to find both the minimum and maximum temperature gradients for concrete and steel superstructures in the United States. The steps for finding the vertical deflections for the 4500 South and I-15 bridge were as follows:

1. Refer to Figure 3.12.3-1 (AASHTO LRFD) – Solar Radiation Zones for the United States. This figure shows all of Utah in zone 1.
2. Refer to Table 3.12.3-1 (AASHTO LRFD) – Basic Temperature Gradients. This table shows that for zone 1, $T_1 = 30^o$ C, and $T_2 = 7.8^o$ C. The values given in this table are for positive temperature gradient only; for the negative temperature gradient values, the first paragraph in section 3.12.3 (AASHTO LRFD) explains that the positive values must be multiplied by -0.30 for plain concrete decks. This gives $T_{1(neg)} = -9^o$ C, and $T_{2(neg)} = -2.34^o$ C.
3. Refer to Figure 3.12.3-2 (AASHTO LRFD) – Positive Vertical Temperature Gradient in Concrete and Steel Superstructures. This figure shows how to assemble the data obtained in steps 1 and 2 into the theoretical temperature gradient. Because the depth of the bridge deck and girder assembly is greater than 400 mm, the dimension (A) is 300 mm. T_3 is assumed to be 0^o C. The positive and negative temperature gradients for the 4500 S. Bridge are shown in Figure 37.

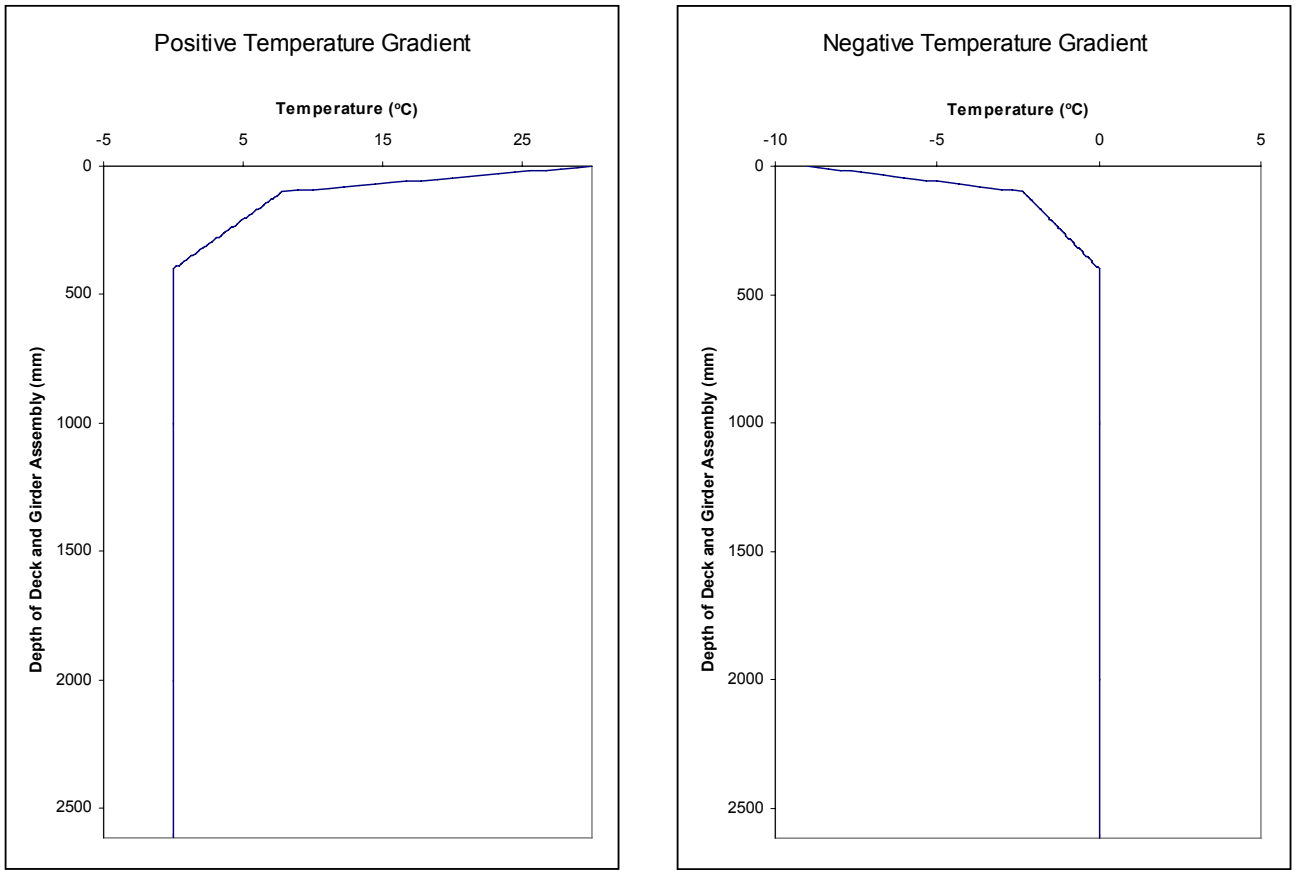

Figure 37. Temperature gradients for calculation of deflection due to thermal effects

The analysis for temperature gradient is found in Section 4.6.6. of the AASHTO LRFD Bridge Design Specifications. The adjacent commentary Section C4.6.6 contains the equations used to find the flexural deformation, or vertical displacements due to the temperature gradient.

$$\varphi = \frac{\alpha}{I_c}\int\int T_g z dw dz = \frac{1}{R} \qquad \text{(C4.6.6-3)} \qquad (17)$$

In the above equation, Φ is the curvature, α is the coefficient of thermal expansion (assumed to be 7.65 x 10^{-6},) I_c is the moment of inertia of the composite concrete section, T_g is the thermal gradient given above, z is the distance to the centroid of the composite deck girder section, and R is the radius of curvature.

Some simplifying assumptions were made in finding the vertical displacement due to thermal gradients. It was assumed that the bridge girder is a simple span with no fixity at the abutments, and the moment of inertia is based upon a concrete section only, and was not transformed for any reinforcing steel. This seemed like a valid assumption because in the above equation only the coefficient for thermal expansion of concrete was used. There was also some question as to the width of the deck section that is assumed to participate as a composite section with the girders. The effective width of the slab used in the calculations was the center-to-center spacing of the girders, which was 3343mm as shown in Figure 38.

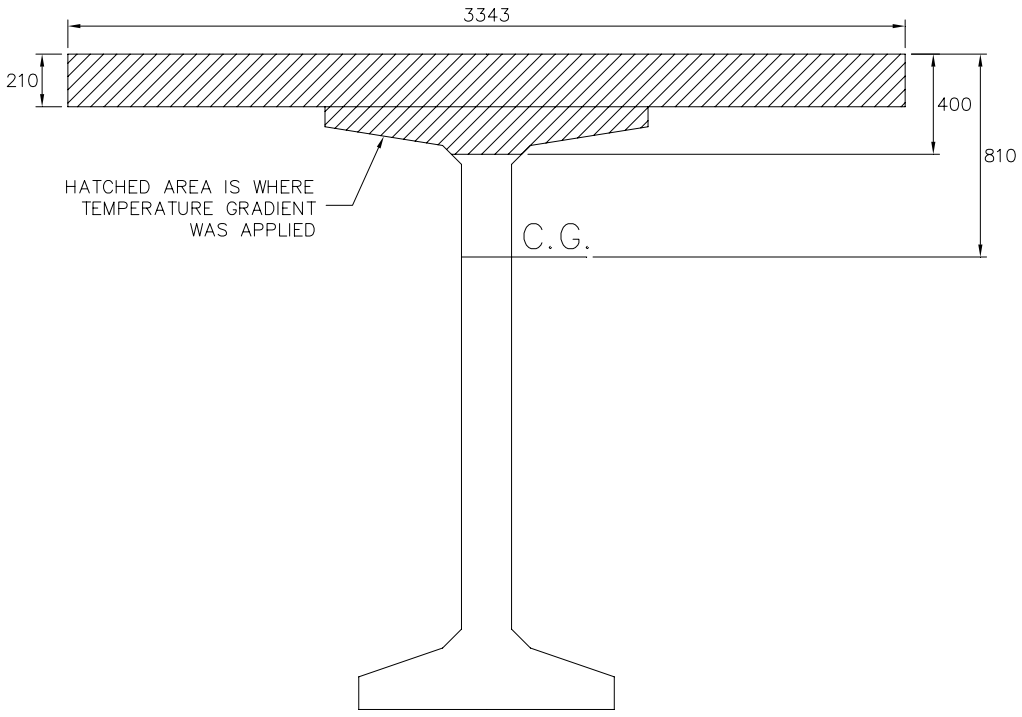

Figure 38. Deck and girder area included in applying thermal gradient

The center of gravity and moment of inertia for the composite deck and girder were calculated by slicing the section vertically into 5mm-thick slices, and using a spreadsheet program to do a summation. The center of gravity was found to be 810mm from the top of the deck, as shown in Figure 38, and the moment of inertia was estimated to be 1.29 x 10^{12} mm^4.

With the moment of inertia and the center of gravity thus obtained, equation C4.6.6-3 was applied in the same manner to each slice, and the summation taken to estimate the curvature for both the positive and the negative temperature gradients. The curvature was then applied to the full span of the girder as a uniformly distributed load, and the bending moment calculated at many points along the span to give both positive and negative deflections due to temperature gradient, using the conjugate beam method. The curvatures found were as follows:

$$\varphi_{(pos)} = 4.11\times10^{-8}/\text{mm} \qquad \varphi_{(neg)} = -1.23\times10^{-8}/\text{mm} \tag{18}$$

Figure 39 shows the negative deflection due to temperature effects expected during the cold winter months, the positive deflection due to temperature effects expected during the hot summer months, and the difference between the two. The difference between the two deflections is the total AASHTO predicted deflection difference that should occur each year.

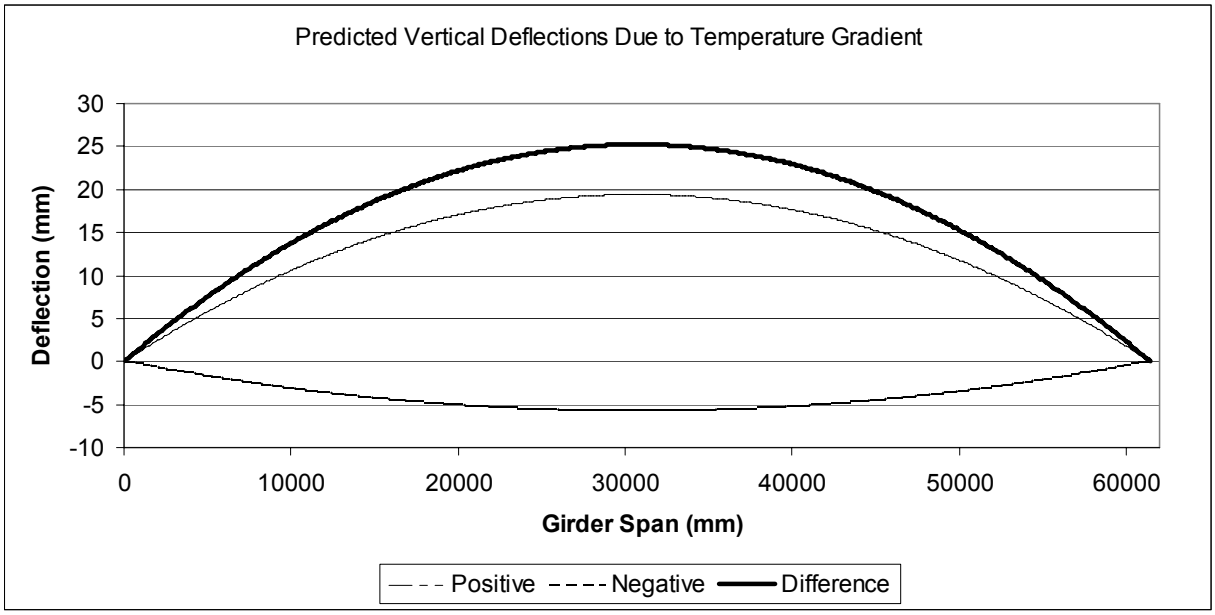

Figure 39. AASHTO prediction for positive deflections, negative deflections, and their difference due to temperature gradient

To compare the AASHTO predicted deflection difference with the actual deflection differences, survey data from 2003 and 2004 was used. A survey of several points along the span of the bridge was taken every two months for several years. The data most useful for this analysis is the 2003 and 2004 data since most if not all of the creep, shrinkage, and post-tensioning losses had occurred. This means that the survey data is only measuring, as closely as possible, the deflections due to temperature.

Figure 40 shows how the actual measurements compare to the predicted deflection. Because the survey was done every two months, there is no data available for January and July as the AASHTO LRFD Code requires. Also, some of the August data was deemed unreliable, therefore, February and June of 2003 and 2004 are the most reliable data for cold and hot months.

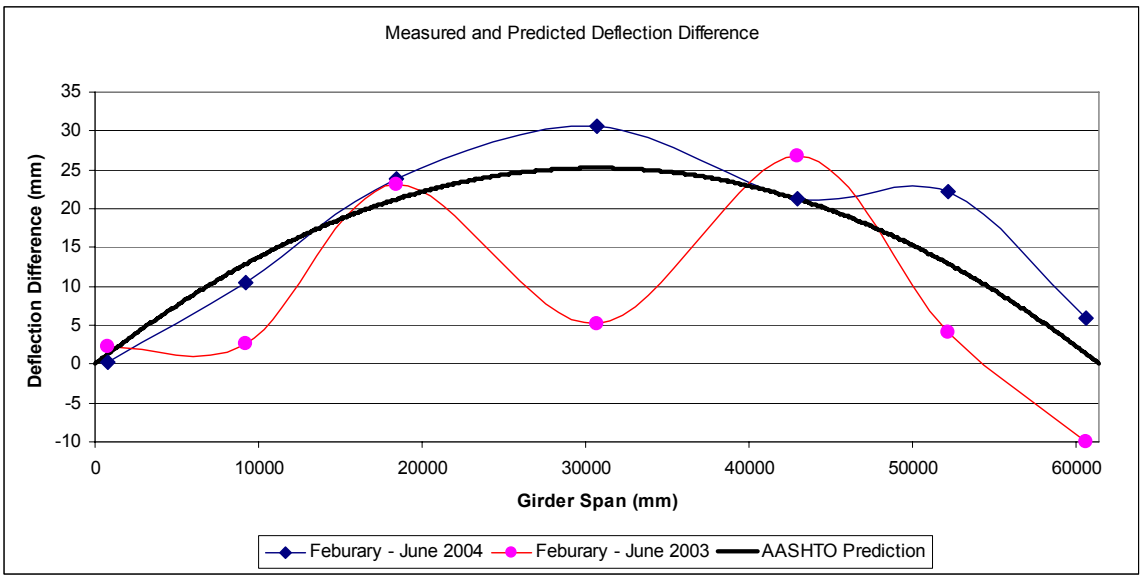

Figure 40. Comparison between AASHTO calculated temperature gradient deflection and measured deflection difference for two periods

Because the predicted deflection is only 25mm over a 61m span, the measurements could have easily been influenced by any number of factors, but the basic trend seems to follow the AASHTO LRFD prediction within approximately 20%. Following the above procedure, the deflections due to thermal temperature gradients of similar girders in other bridges can be determined.

13. MEASUREMENT OF ABUTMENT MOVEMENTS AND ROTATIONS

The best data obtained for showing the movement of the abutments is the survey data between August 2002, and August 2004. There are survey targets on girder lines G1, G5, and G8. These are counted from east to west on the northbound bridge, as shown in Figure 41.

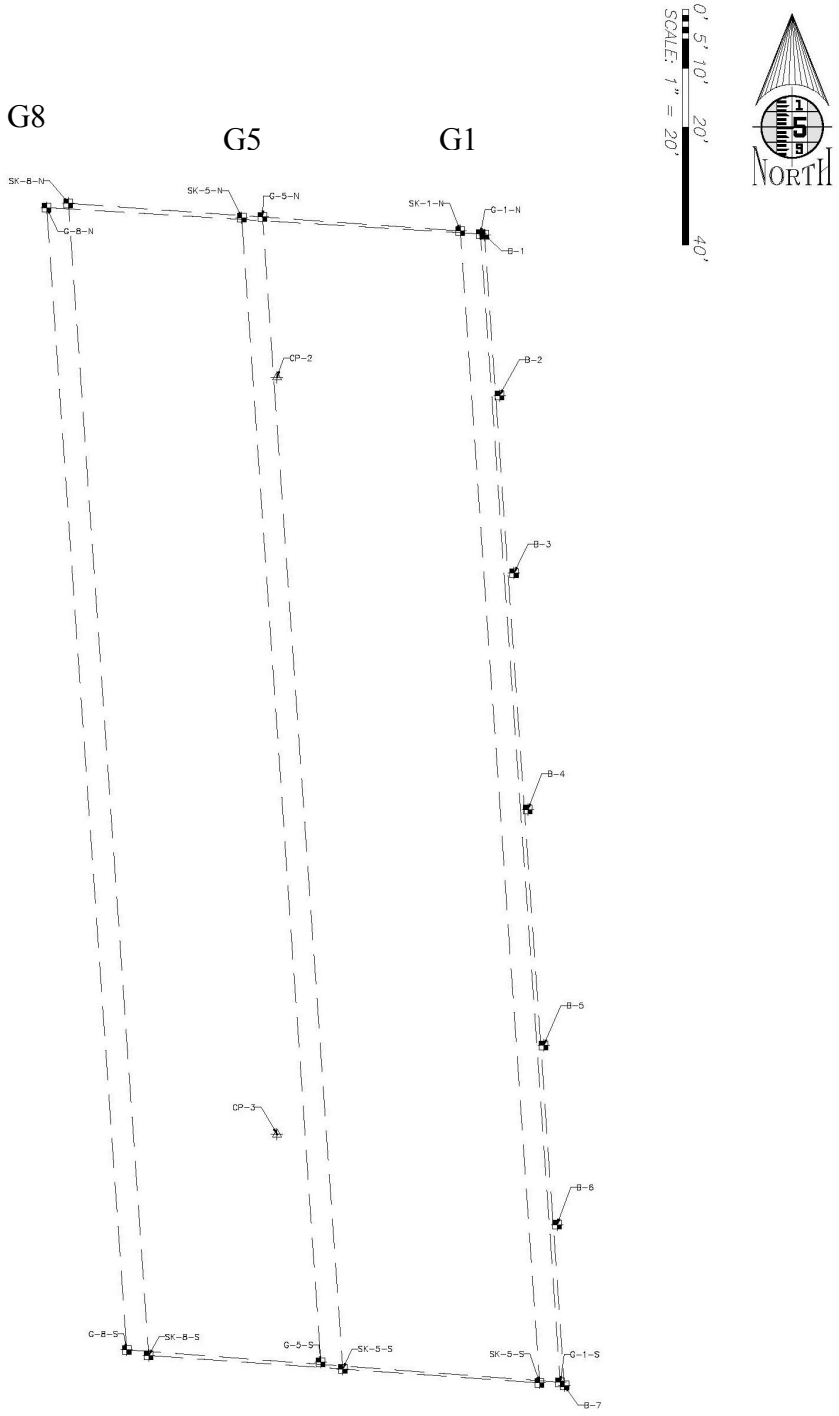

Figure 41. Survey targets on girders G1, G5 and G8 for measuring movement of abutments.

In order to justify applying any of this data to the abutments, observations were made at the bridge, and it was determined that the girder targets closest to the abutments are a fair representation of the abutments themselves. Figure 42(a) is a photograph of a typical joint where the girders are embedded into the abutments. Because of the design of the abutments, and the anchorage of the girder ends into them, it appears that the girders have remained securely attached to the abutments, and any measured movement of the ends of the girders is shared with the abutment it is embedded into. There is no observed relative movement between the girders and the abutments. Figure 42(b) shows the survey targets on the bottom girder flanges and abutments.

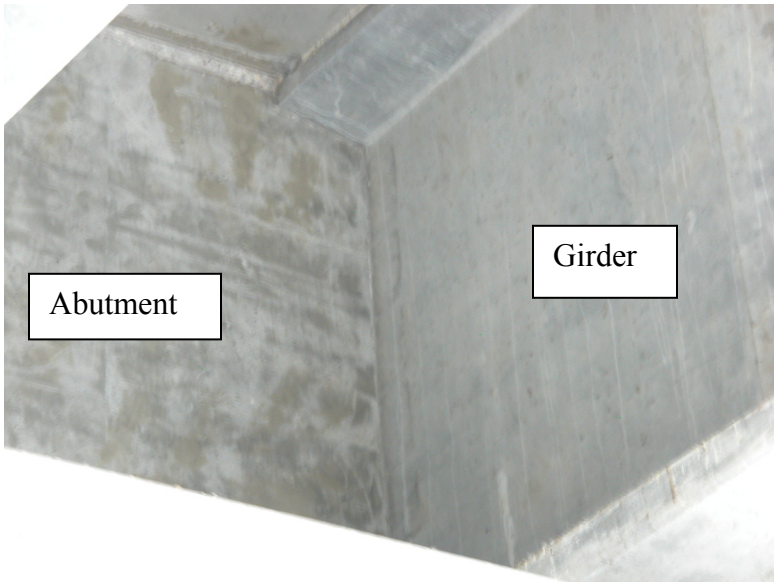

(a)

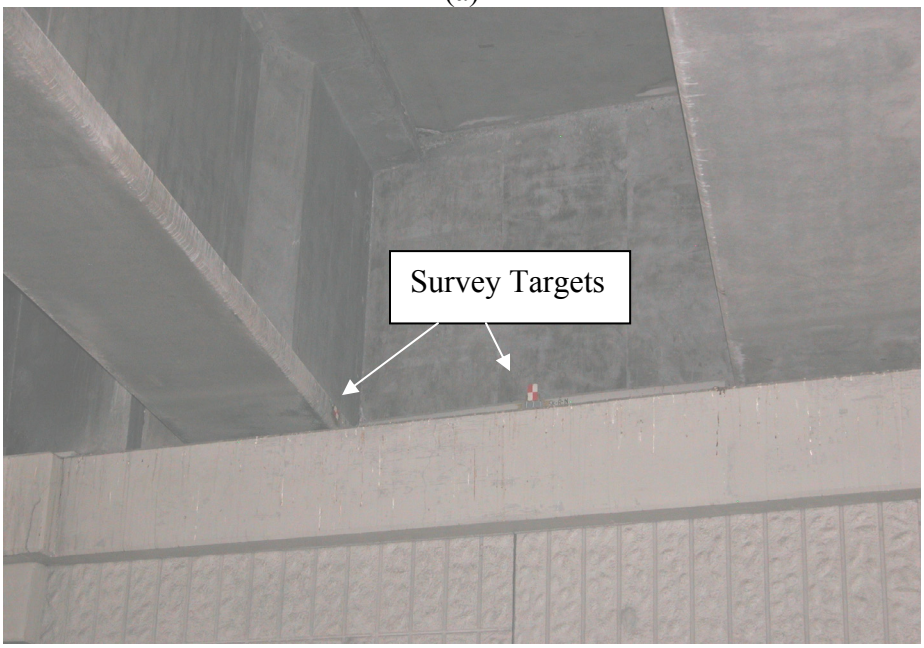

(b)

Figure 42. Connection between girders and north abutment: (a) detail, (b) survey targets

Some of the survey data reported appears to be erroneous, and was therefore eliminated. Also, in an attempt to make any trends more visible, and the plots easier to read, some of the repetitive data was also eliminated.

Figure 43 and 44 show plots of transverse and longitudinal translations of the North and South abutments, respectively. These plots were obtained by taking the first survey points (Aug-2002) as baseline points, and showing the East-West transverse translation exaggerated. The actual distance between girders G1, G5, and G8 is shown on the secondary axis. Therefore, values on the main East-West axis do not represent absolute translations. It is observed that the maximum relative translation in the North abutment is 47 mm (1.85 in.) in the north-south direction approximately at girder G5. The maximum relative translation in the South abutment is 40 mm (1.57 in.) in the north-south direction approximately at girder G8. The maximum relative translation in the east-west direction of 19 mm (0.75 in.) occurs at the South abutment near girder G1.

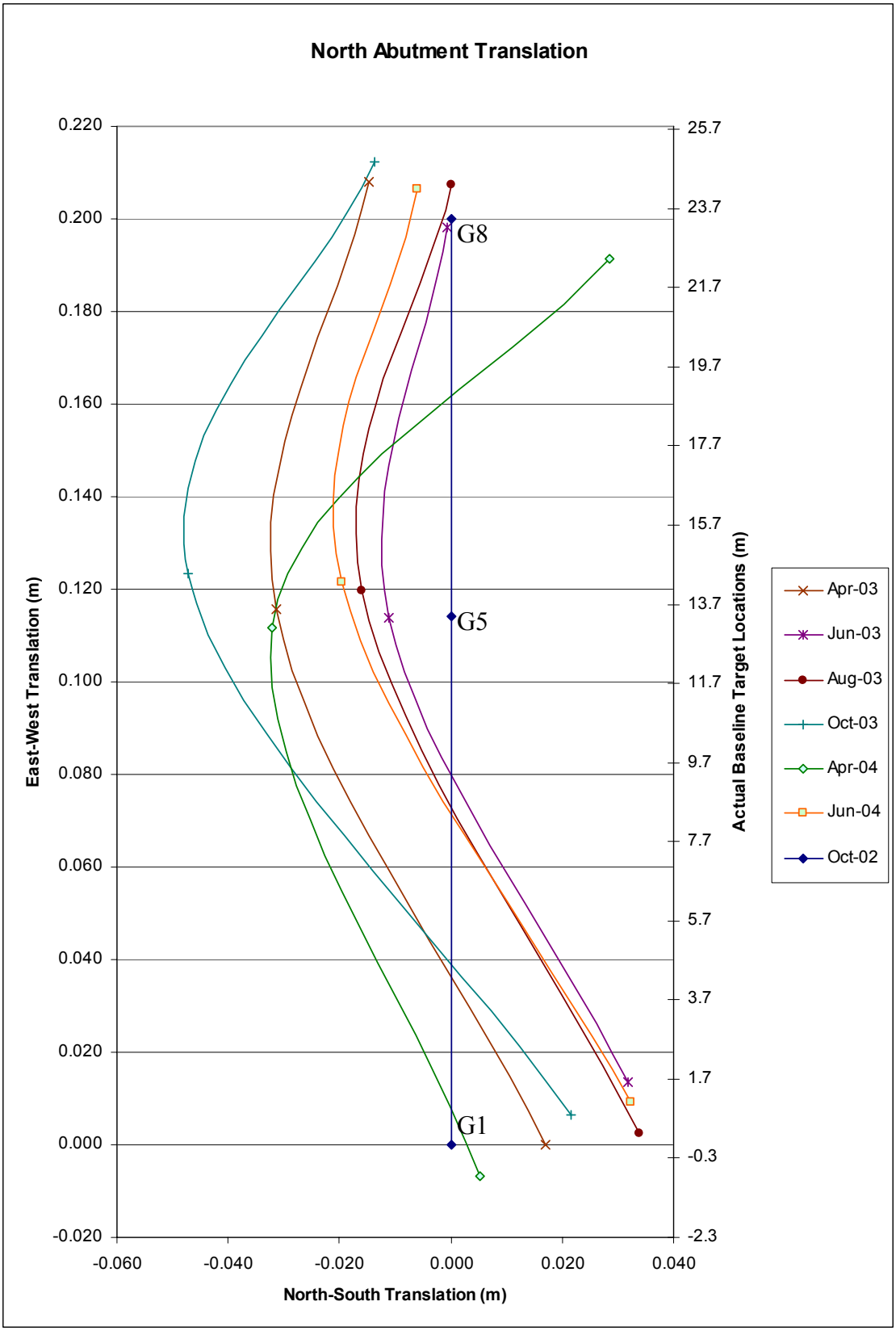

Figure 43. North abutment translation.

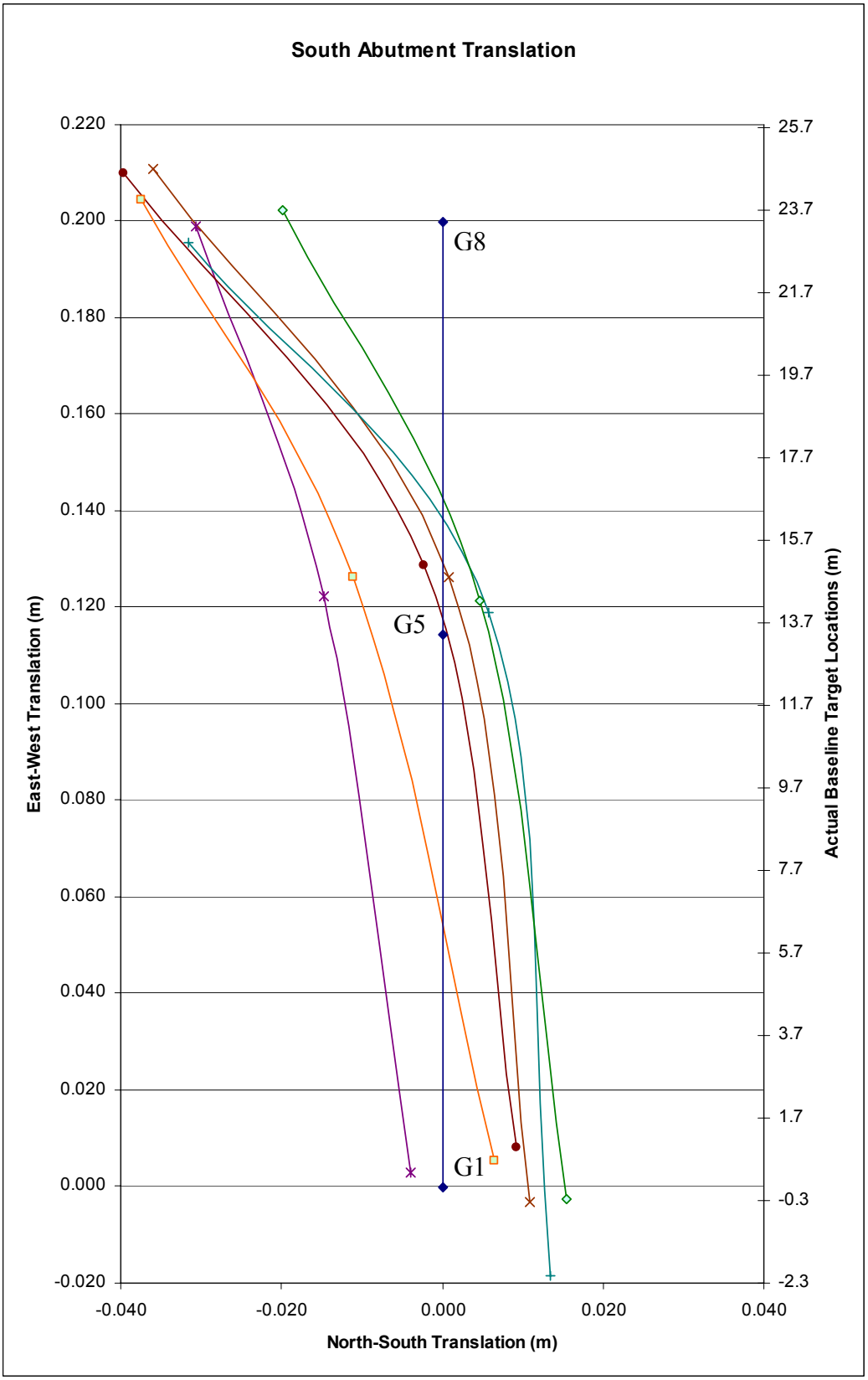

Figure 44. South abutment translation. (See legend in Figure 43)

The vertical movements of the abutments are shown in Figures 45 and 46, which were obtained in much the same manner as Figures 43 and 44. The settlements shown are actual absolute settlements over the period of time given in the plots, but the East-West transverse translation values given in the figures do not represent absolute translations and must be obtained by subtracting the baseline values. It can be observed that the maximum settlement in the North abutment is 21 mm (0.83 in.) approximately at girder G5. The maximum settlement in the South abutment is 8 mm (0.31 in.) approximately at girder G1. The maximum relative translation in the east-west direction of 19 mm (0.75 in.) occurs at the south abutment near girder G1. The bridge is in constant movement, and this data may serve to provide designers with a good idea of what kind of sustained movement to expect in order to improve the design of the approaches and shear key tolerances for bridges built in similar soil and weather conditions.

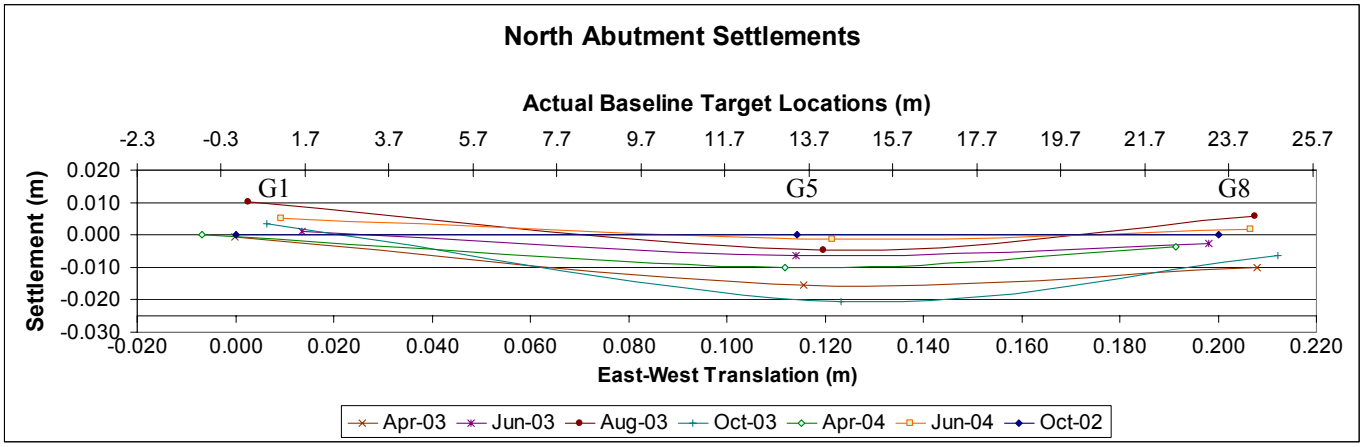

Figure 45. North abutment vertical settlement.

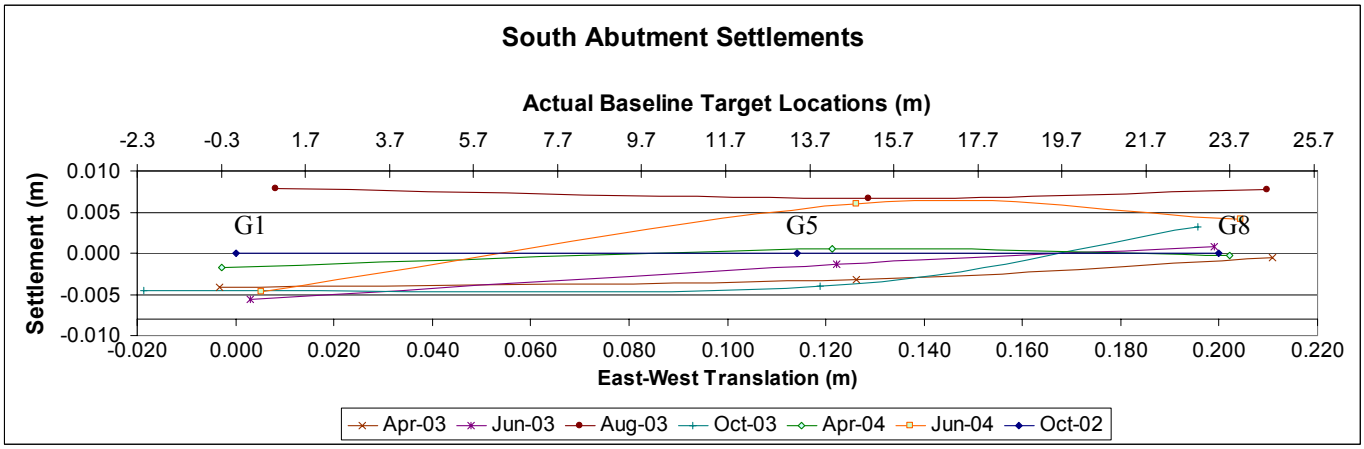

Figure 46. South abutment vertical settlement.

Abutment rotations were obtained by approximating them by the girder end rotations. It has been observed that the girders and abutments are fixed to each other. This joint has shown no sign of movement, therefore, the assumption has been made that the abutment rotations are equal to the girder end rotations. The cambered shape of the girders closely resembles a parabola. The girder end rotations were approximated by curve fitting a parabola to the cambered shape of the girder and finding the equation for the parabola at each measurement. With the equation thus obtained, the slope is easily found by taking the first derivative and setting it equal to zero, for the location where the slope is required. The abutment rotations are observed to be small enough, that the slope is also equal to the angle in radians. Figure 47 shows the slope of the girder ends over approximately a two year period. The abutment end rotation in that time ranges from 0.00545 to 0.00605 radians (0.31 to 0.35 degrees), which appears to be almost negligible.

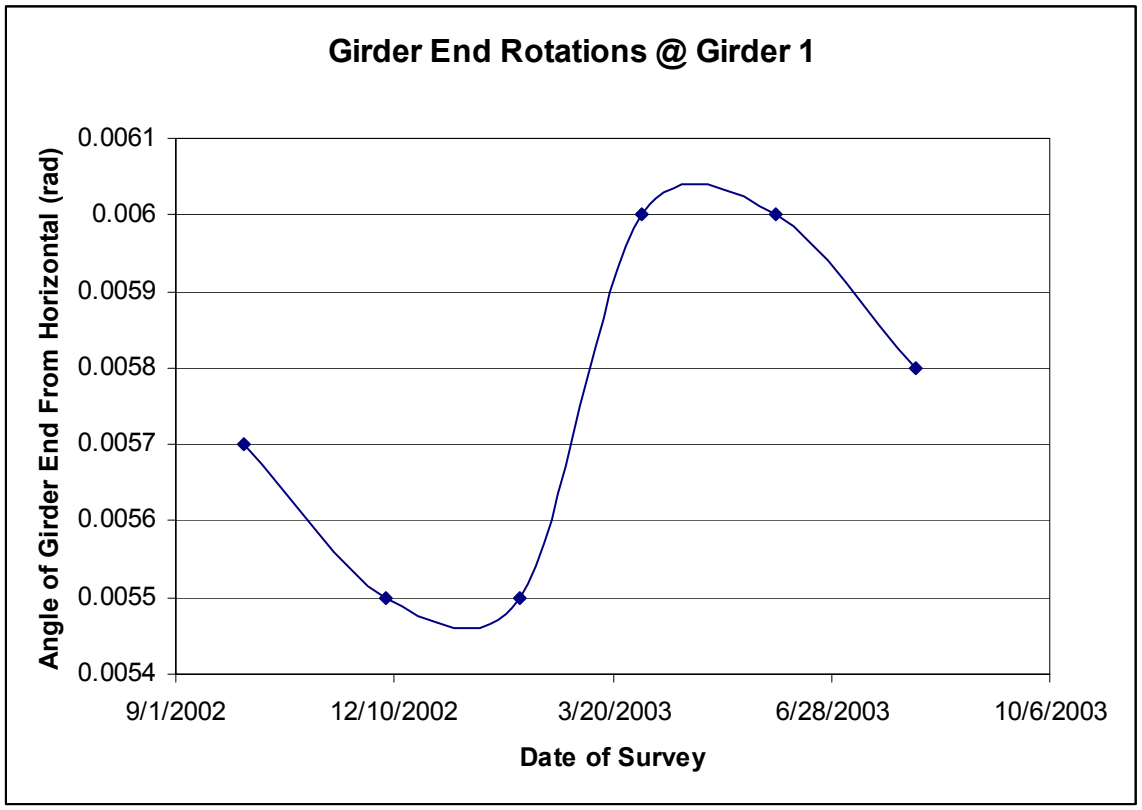

Figure 47. Girder end rotations for girder G1.

14. SUMMARY AND RECOMMENDATIONS

The bridge being monitored consists of eight spliced, post tensioned, precast concrete girders, having three segments each, for a single clear span of 61.443 m (201 ft-7 in.). The bridge has been monitored for a period of 1342 days. Survey measurements confirm that the elevations of the north and south splice points have not varied by more than 4 mm (0.16 in.) from each other, and on average the splice points have varied by only 1 mm (0.04 in.). The coincidence of the splice points relative to each other indicates excellent girder/splice performance. The south–end abutment has experienced a settlement of 38 mm (1.5 in.), while the north-end abutment has experienced 20 mm (0.8 in.) of settlement. The deflected shape of the easternmost spliced girder is approximately parabolic, and the absolute upward midspan deflection has stabilized to approximately 0.15% of the clear span.

Compressive strains increased due to creep and shrinkage of concrete but reached equilibrium eight months after post tensioning, as observed from vibrating wire strain gauges embedded in the concrete. This observation was confirmed by examination of creep and shrinkage strains from creep and shrinkage tests of identical concrete cylinders. Concrete strains after this time have come to equilibrium and only seasonal temperature-related strains are observed.

Comparison of the strains measured across the splice points in the eastern-most girder with those of girder segments in three other girders shows that the strains are uniform. This indicates that the two splice diaphragms are performing well in their task of maintaining continuity between the precast concrete girder segments, and among the various girders of the bridge. This uniformity and consistency among the girders indicates a lack of differential displacement at the splice diaphragms and excellent diaphragm action.

Tendon losses of the eastern-most spliced girder were measured using eight load cells at the abutments in the anchorage zones. The measured time-dependent losses from Tendons #1, #2 , and #3 ranged from 13% to 17%, with the top tendon (Tendon #1) having the largest loss. After 3 years and 8 months the average losses at midspan are 14.5% based on vibrating wire strain gauge readings.

After 3.7 years, computations using the AASHTO LRFD time-dependent method at the jacking and anchored end of the anchorage zones, and at midspan predict a higher remaining prestressing force at the bottom tendon compared to the top tendon, which is confirmed by the measurements from the load cells at the anchorage zones and the vibrating wire strain gauges at midspan. The AASHTO LRFD time-dependent method predicted the total losses in the range of 14% to 23% at the jacking end, and 15% to 25% at the anchored end of the anchorage zones; the load cell measurements at the jacking end ranged between 14% and 17%, and at the anchored end they ranged between 13% and 15%. The AASHTO LRFD time-dependent method predicted the losses in the range of 15% to 22% at midspan, whereas the vibrating wire strain gauge measurements show losses in the range of 14% to 15% at midspan. The time-dependent method predicts the measured losses with sufficient accuracy, it is conservative for all locations, and compares favorably to the experimental measurements.

The research has shown that overall, the spliced-girder bridge system as designed is performing very well. It is providing the single clear span as intended with predictable performance and serviceability. No cracking in any of the girders has been observed; in the girder axis direction no tensile strain was observed. The design of the spliced-girder bridge system was carried out adequately regarding the issue of losses for the post-tensioned girders.

Therefore, the use of spliced post-tensioned girders as designed in this project is recommended for constructing similar spliced-girder bridges.

Shrinkage and creep tests were performed on samples of concrete used in constructing the post-tensioned spliced, precast concrete girders under investigation. From the tests performed in this study, the recommended value of the ultimate shrinkage strain for a concrete age 3 days is 780×10^{-6}. The recommended value of ultimate creep coefficient from this study for a concrete age of three days is 2.16. The shrinkage and creep tests indicate an asymptotic achievement of ultimate shrinkage and creep in approximately eight months. This is supported by strain readings from vibrating wire strain gauges embedded in the concrete of the spliced, precast concrete girders being monitored. The concrete modulus of elasticity was overestimated by ACI-318 but was predicted in a satisfactory manner by the ACI 363 expression.

LVDT measurements at the cold joints under the deck in truck load tests and from ambient measurements show that the range of displacements is between 15-21 thousands of an inch (0.38 mm – 0.53 mm). Thus, the cold joints are believed to be in good health. Moreover, the lack of deck cracking in this bridge as compared to the decks of steel girder bridges makes this a successful system. During observations under rainy conditions, no water was observed below the deck. Therefore, it is recommended that the use of precast concrete panels for constructing the deck be continued.

The abutment movements and rotations were obtained from measurements carried out by surveys and were found to be small. It was observed that the maximum north-south relative translation was in the North abutment and was equal to 47 mm (1.85 in.). The maximum relative translation in the east-west direction was 19 mm (0.75 in.) and occurred at the South abutment. The maximum settlement was in the North abutment and was equal to 21 mm (0.83 in.). The abutment rotations were approximated by the girder end rotations and were found to be in the range from 0.00545 to 0.00605 radians (0.31 to 0.35 degrees).

The original design of the girders assumed a total loss of prestress of 27,000 psi (186 MPa). This is a loss of 13.3% from the original post-tensioning jacking stress of 202.5 ksi (1396 MPa). The measured losses were 13.4% for the anchored end, 14.9% for the jacking end and 14.5% for midspan. As can be seen the assumed losses were very close to those observed and the design methodology for incorporating losses is adequate.

The vertical deflections of the post-tensioned girders under monitoring were measured due to thermal gradients and were compared to AASHTO predicted deflections. The predicted deflection was only 25mm (0.98 in.) over the 61.443 m (201 ft-7 in.) span, and it closely followed the measured deflections. It is therefore believed that the AASHTO method is reliable for prediction of deflections due to thermal gradients for spliced post-tensioned girder bridges.

The research has shown that in general the spliced-girder post-tensioned bridges are a superior system and should be seriously considered in future projects. It is recommended that in future projects the abutment and girder movements be taken into account when designing the shear keys. Observations and measurements made for the 4500 South Bridge contained in this report could be used as a guideline.

Another issue that has come out of the report is the amount of required camber of the post-tensioned girders. The deflection data provided in the present report should be taken into consideration when calculating the required camber for such post-tensioned spliced girders in future projects.

15. NOTATION

A_c = area of concrete girder section;

E_c = modulus of elasticity of concrete;

E_{ci} = modulus of elasticity of concrete at transfer;

E_{ps} = modulus of elasticity of prestressing reinforcement;

e = eccentricity of the tendon;

f_c' = concrete compressive strength;

f_{cs} = stress in the concrete at the level of the centroid of the prestressing tendons;

f'_{pi} = initial stress in prestress steel;

f_{py} = yield strength of prestressing steel;

f_{pu} = specified tensile strength of prestressing steel;

H = average annual ambient relative humidity;

I_c = moment of inertia of the girder section;

j = number of jacking operations;

L = tendon length;

L_g = girder span;

M_D = bending moment due to the total superimposed load;

N = number of identical tendons (four);

P_i = axial load;

r = radius of gyration of the girder section;

t = time (days);

t_i = age of concrete when load is initially applied (days);

t = time (hours);

V / S = volume-to-surface ratio;

w_c = concrete unit weight;

x = length of a prestressing tendon from the jacking end to any point under consideration;

y' = total vertical change of tendon path;

α = sum of the absolute values of angular change of prestressing steel path from jacking end to the point under investigation;

γ_c = creep coefficient;

γ_{sh} = shrinkage coefficient;

(γ_{la}) = loading age adjustment factor;

γ_λ = shrinkage (creep) correction factor for humidity;

γ_{VS} = shrinkage (creep) correction factor for volume to surface ratio;

$\Delta f_{CR}(t)$ = loss due to creep of concrete;

Δf_{ES} = loss due to elastic shortening;

$\Delta f_R(t)$ = loss due to relaxation of steel after transfer;

$\Delta f_{SH}(t)$ = loss due to shrinkage;

$(\varepsilon_{sh})_t$ = time-dependent shrinkage strain;

$(\varepsilon_{sh})_u$ = ultimate shrinkage strain;

K = wobble friction coefficient per unit length of tendon;

k_c = creep factor for the effect of volume-to-surface ratio;

k_f = creep factor for the effect of concrete strength;

k_h = shrinkage factor for the effect of humidity;

k_s = shrinkage factor for the effect of volume-to-surface ratio;

μ = coefficient of friction;

v_t = time-varying creep;

v_u = ultimate creep coefficient;

$\psi(t,t_i)$ = time-dependent creep coefficient;

16. REFERENCES

AASHTO Subcommittee on Bridges and Structures (1975), "Interim Specifications – Bridges," American Association State Highway and Transportation Officials, Washington, D.C., pp. 41-79.

AASHTO (2004), "AASHTO LRFD Bridge Design Specifications," *American Association of State Highway and Transportation Officials*, Third Edition, Washington, D.C.

Abdel-Karim, A.M. and Tadros, M.K. (1992), "Design and construction of spliced I-girder bridges," *PCI Journal*, Vol. 37, No. 4, July-August, pp. 114-122.

Abdel-Karim, A. M. and Tadros, M.K. (1993), "Computer Analysis of Spliced Girder Bridges," *ACI Structural Journal*, Vol. 90, No. 1, Jan. - Feb., pp. 21-31.

American Concrete Institute-American Society of Civil Engineers Joint Committee 323 (1958), "Tentative Recommendations for Prestressed Concrete," ACI Journal Proceedings, Vol. 54, No. 1, January, 545-578.

American Concrete Institute (1997), "ACI Committee 209. Prediction of Creep, Shrinkage, and Temperature Effects in Concrete Structures. (ACI 209R-92 Reapproved 1997)," *American Concrete Institute*, Detroit, Mich.

American Concrete Institute (1997), "ACI Committee 363. State-of-the-Art Report on High-Strength Concrete. (ACI 363R-92 Reapproved 1997)," *American Concrete Institute*, Detroit, Mich.

American Concrete Institute (2005), "ACI Committee 318. Building Code Requirements for Structural Concrete. (ACI 318-05) and Commentary (ACI 318R-05)," *American Concrete Institute*, Farmington Hills, Mich.

American Society for Testing and Materials (1994), "C469-94 Standard Test Method for Static Modulus of Elasticity and Poisson's Ratio of Concrete in Compression," *American Society for Testing Materials*, Vol. 04.02, West Conshohocken, Pa.

American Society for Testing and Materials (1994), "C512-87(1994) Standard Test Method for Creep of Concrete in Compression," *American Society for Testing Materials*, Vol. 04.02, West Conshohocken, Pa.

American Society for Testing and Materials. ASTM C 39 (1999), "C39/C39M-99 Standard Test Method for Compressive Strength of Cylindrical Concrete Specimens," *American Society for Testing Materials*, Vol. 04.02, West Conshohocken, Pa.

Branson, D.E. and Kripanarayanan, K.M. (1971), "Loss of Prestress, Camber and Deflection of Non-Composite and Composite Prestressed Concrete Structures," *PCI Journal*, Vol. 16, No. 5, September-October, 22-53.

Collins, M., and Mitchell, D. (2003). *Prestressed Concrete Structures.* Response Publications, Canada.

Geren, K. L. and Tadros, M. K. (1994), "The NU Precast/Prestressed Concrete Bridge I-Girder Series," *PCI Journal*, Vol. 39, No. 3, May-June, pp. 26-39.

Meyers, B.L.; Branson, D.E.; and Schumann, C.G. (1972), "Prediction of Creep and Shrinkage Behavior for Design from Short Term Tests," *PCI Journal*, Vol. 17, No. 3, May – June, 29-45.

Nawy, E.G. (2003), *Prestressed Concrete: A Fundamental Approach,* Prentice Hall. Upper Saddle River, New Jersey.

Oh, B.H. and Yang, I.H. (2001), "Realistic Long-Term Prediction of Prestress Forces in PSC Box Girder Bridges," *ASCE Journal of Structural Engineering*, Vol. 127, No. 9, pp. 1109-1116.

PCI Committee on Prestress Losses (1975), "Recommendations for Estimating Prestress Losses," *PCI Journal*, Vol. 20, No. 4, Jul.-Aug., pp. 43-75.

PCI (2004), "PCI Design Handbook: Precast and Prestressed Concrete," 6th Edition, PCI, Chicago, Ill.

Ronald, H.D. (2001), "Design and Construction Considerations for Continuous Post-Tensioned Bulb-Tee Girder Bridges," *PCI Journal*, Vol. 46, No. 3, May-June, pp. 44-66.

Seguirant, S.J. (1998), "New Deep WSDOT Standard Sections Extend Spans of Prestressed Concrete Girders," *PCI Journal*, Vol. 43, No. 5, July-August, pp. 92-119.

Stallings, J.M.; Barnes, R.W.; and Eskildsen, S. (2003), "Camber and Prestress Losses in Alabama HPC Bridge Girders," *PCI Journal*, Vol. 48, No. 5, September-October, pp. 90-104.

Tadros, M.K.; Ghali, A.; and Dilger, W.H. (1975), "Time-Dependent Prestress Loss and Deflection in Prestressed Concrete Members," *PCI Journal*, Vol. 20, No. 3, May-June, pp. 86-99.

Tadros, M.K.; Ghali, A.; and Dilger, W.H. (1979), "Long-Term Stresses and Deformation of Segmental Bridges," *PCI Journal*, Vol. 24, No. 4, July-Aug., pp. 66-87.

Tadros, M.K.; Ghali, A.; and Meyer, A.W. (1985), "Prestressed Loss and Deflection of Precast Concrete Members," *PCI Journal*, Vol. 30, No. 1, January-February, pp. 115-141.

Wollmann, G.P.; Anderson, R.B.; and Roberts-Wollmann, C.L. (2003), "Creep and Shrinkage Effects in Spliced Prestressed Concrete Girder Bridges," *PCI Journal*, Vol. 48, No. 6, November-December, pp. 92-105.